Bioinspired & biocompatible coatings of poly(butylene adipate-co-terephthalate) and layer double hydroxide composites for corrosion resistance

Hussain R. Rizvi, B.E

Thesis Prepared for the Degree of

MASTER OF SCIENCE

UNIVERSITY OF NORTH TEXAS

May 2016

Dr. Nandika D'Souza, Major Advisor

Dr. Reza Mirshams, Committee Member

Dr. Seifollah Nasrazadani, Committee Member

Dr. Sheldon Shi, Committee Member

Dr. Tae-Youl Choi, Committee Member

Rizvi, Hussain R. Bioinspired & biocompatible coatings of poly (butylene adipate-co-terephthalate) and layer double hydroxide composites for corrosion resistance. Master of Science (Mechanical and Energy Engineering), May 2016, 63 pp., 6 tables, 25 figures, 64 numbered references.

Hierarchical arrangement of biological composites such as nacre and bone containing high filler (ceramic) content results in high strength and toughness of the natural material. In this study we mimic the design of layered bone microstructure and fabricate an optimal multifunctional bio-nanocomposite having strength, toughness and corrosion resistance. Poly (butylene adipate-co-terephthalate) (PBAT), a biodegradable polymer was used as a substrate material with the reinforcement of LDH (Layered double hydroxide) as a nanofiller in different concentrations to achieve enhancement in mechanical properties as well as processing related thermostability. Corrosion resistance was increased by mimicking a layered structured which incorporated a tortuous diffusion path.

Copyright 2016

by

Hussain R. Rizvi

ACKNOWLEDGEMENTS

I would like to thank my advisor Dr. Nandika D'Souza for the continuous support of my M.S. study and research. Her motivation, immense knowledge, and guidance have provided me with a unique skill set to excel in any endeavor.

I would also like to thank the commettiee members Dr. Sheldon Shi, Dr. Tae-Youl Choi, Dr. Reza Mirshams and Dr. Seifollah Nasrazadani for their guidance, encouragement and suggestion in nanoindentation and corrosion study.

My special thanks to my lab mates Dr. Mangesh Nar, Andres Garcia, Yoni Mercier, Nathan Warner, Zachary Hoyt and Changlei Xia for their assistance and support from the very first day that help me to complete this thesis.

CONTENTS

LIST OF TABLES

LIST OF ILLUSTRATIONS

CHAPTER 1

INTRODUCTION

Multifunctional properties of the Biological structures have always been a source of inspiration. These structures are engineered in a complex hierarchical design, which gives unique functionality at nanoscale and structured in a recurring pattern to give exceptional structural properties at macroscale. Material properties of the individual constituent of the natural material are significantly less as compared to the macrostructure that is built up from these constituent. This unique characteristics of hierarchical biological structures have created interest in bioinspired materials design. Natural composites can be categories depending upon the percentage of the mineral and polymeric content into three divisions. First one is the materials that contain very higher content of mineral such as bone, teeth and seashell. Second category includes materials that have lower percentage of mineral in it, this category include structures such as fish scales and lobster cuticle. Third one are the structures that are purely polymeric that includes wood, bamboo and silk. [1] Hence, mimicking the design of natural material incorporate numerous potential. Materials with multifunctional characteristics can be created that are strong, tough and damage intolerant which can be used for different applications.

In this thesis, materials from first category i.e. containing high percentage of minerals is mimic. The effect of higher filler content on mechanical, thermal and electrochemical properties of the composites are studied.

1.2 Biological Composites:

Bone and nacre are the leading examples of biological materials that are structured in a manner that have increase their strength and toughness making them hard to damage [1]. Ninety five percent of bone dry weight is composed of two main molecules. Collagen molecule that are around 300 nm long and about 1.5nm in diameter fibrils and hydroxyapatite nanoparticles $Ca_{10}(PO_4)_6(OH)_2$ having dimensions of 50 nm × 25 nm and 1.5-4 nm thick. The nanoparticles are arranged along the collagen fibrils in a hierarchical structured network which give the strength and toughness both at the macro scale. [2]

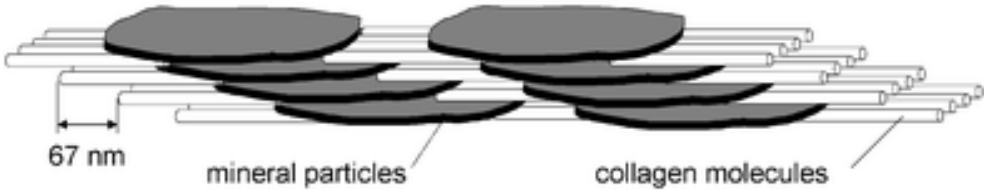

Figure 1. 1 Structural arrangement of mineral and collagen molecules in bone. [3]

Nacre on the other hand consist of Brick and mortar arrangement. Aragonite (Calcium Carbonate) platelets having thickness of 200-900 nanometer and diameter of 5-8 micrometer acts as bricks. These platelets are joined together by a thin organic matrix of elastic biopolymer such as chitin. The brick wall structure of the aragonite results in a 40 fold increase in toughness. The fracture toughness of nacre is about 10 MPa $m^{1/2}$ whereas for aragonite is about 0.25 MPa $m^{1/2}$ [4]. Almost 2000 times more fracture resistant than the constituent mineral. Hence, mimicking the biological structure

is a reasonable approach, which leads to the structure that have high strength as well as they are tough.

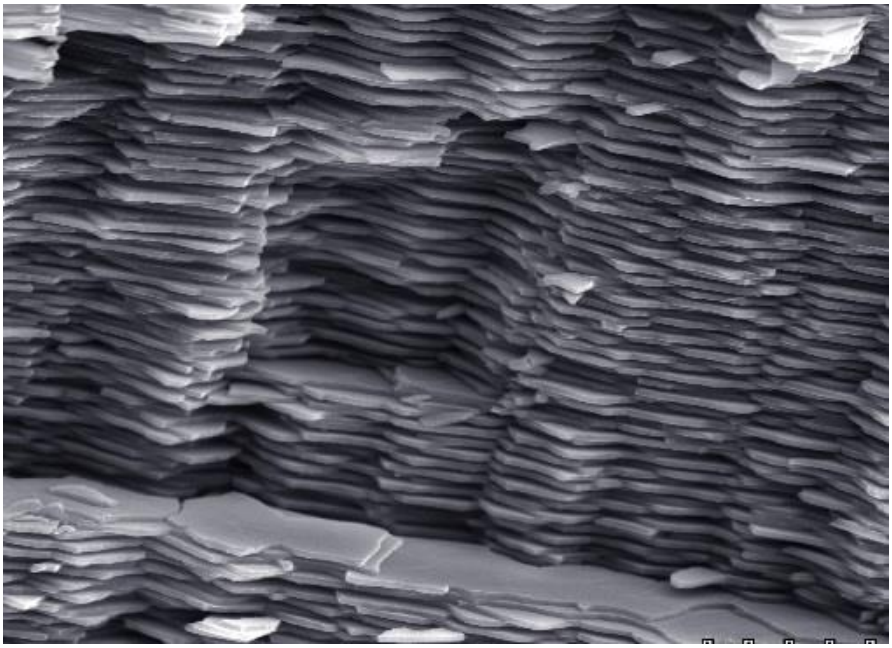

Figure 1. 2 Structural arrangement of aragonite mineral to form nacre brick and mortar microstructure [5].

1.3 Implantable Materials

Human Implants consists mainly of materials such as Titanium alloys, cobalt-chromium and 316L stainless steel, because of the high mechanical properties and their adaptability within the physiological environment. One of the main shortcoming of metallic implant is the compatibility with the ionic tissue environment resulting in the corrosion or encapsulation of the implant by the fibrous tissue. Stainless steel is mostly prone to corrosion and is use for time limited application. Moreover the diffusion of the metallic ions through the oxide layer of the implants accumulates in the tissue resulting in the layer of fibrous tissue whose thickness is proportional to the amount and toxicity of the dissolution material. Hence various deposition techniques such plasma spraying, sol-gel, Chemical vapor deposition, Physical vapor deposition and PLD (Plasma laser deposition) are being used to modify the surface of the implant. Each technique has its own advantages and drawbacks with varying coating thickness. The coatings or surface treatments methods are applied to overcome the ion release, corrosion, wear and tear, but also to improve functionality of the implant by incorporating drug to the surface for control release [6] [7]. Polymeric coatings are mainly used to improve the corrosion resistance [8] and to serve as a drug carrier for controlled release [9]. Also, one important parameter for any implantable material is biocompatibility which is being tested according to biological evaluation the medical devices (ISO 10993) standards to check the cytotoxicity and hemocompatibility of the implantable object.

Figure 1.3 Human Implant (a) Stent [10] (b) Knee joint [11] (c) Ball and socket joint, hip implant [12] (d) Heart valve [13].

1.4 PBAT:

PBAT is an aliphatic-aromatic co-polyester. It is a result of poly-condensation of 1,4-butanediol and a mixture of adipic acid and terephtalic acid [14]. In an aliphatic aromatic co-polyester, aromatic part of chain provide strong physical and mechanical properties. Nevertheless they also provide resistance to microbial attack resulting in the lower degradability [15]. The biodegradability of the mainly due to the presence of aliphatic polyesters. Hence higher the ratio of aromatic unit results in higher mechanical and microbial resistant properties [16]. In PBAT, butylene adipate group provide the biodegradability when composted while the terephthalate provide stability and high mechanical properties [17]. It has high flexibility about 700% at break and also ease in processibility. The chemical structure of PBAT is given in the figure 1.4.

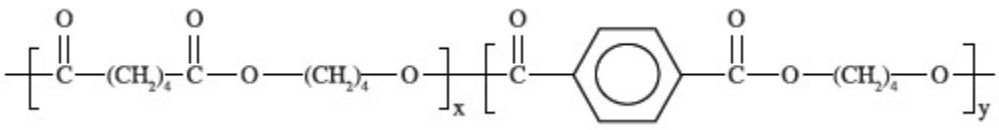

Figure 1. 4 Chemical structure of poly (butylene adipate-co-terephthalate).

One important parameter to consider for implant coating application is the biocompatibility of the material. Fukushima et al. tested the PBAT and clay contents for in vitro cytotoxicity, protein adsorption and hemocompatibility. Results showed PBAT to be biologically safe and does not affect the blood cell count [18].

Table 1: Material and mechanical properties of blown film of PBAT*

Property	Unit	Test Method	PBAT Ecoflex®
Mass density	g/cm3	ISO 1183	1.25 – 1.27
Melt flow rate MFR 190 °C, 2,16 kg	g/10 min	ISO 1133	2.7 – 4.9
Melt volume rate MVR 190 °C, 2,16 kg	ml/10 min	ISO 1133	2.5 – 4.5
Melting point	°C	DSC	110 – 120
Shore D hardness	–	ISO 868	32
Vicat VST A/50	°C	ISO 306	91
Transparency	%	ASTM D 1003	82
Tensile strength	N/mm^2	ISO 527	35/44
Ultimate strength	N/mm^2	ISO 527	36/45
Ultimate Elongation	%	ISO 527	560/710
Failure Energy (Dyna Test)	J/mm	DIN 53373	24
Permeation rates: Oxygen (23°C, dry)	$cm^3/(m^2*d*bar)$	ASTM D 3985	1200
Water vapour (23°C, 85 % r.h.)	$g/(m^2*d)$	ASTM F-1249	135

*Material properties are adopted from supplier's website.

1.5 LDH:

Layered double hydroxides (LDHs) are layered mineral also called anionic clay having positively charged brucite type layers of divalent and trivalent metal hydroxides. Negatively charged ions mostly carbonate are present between the metallic layers to balance the positive charge of the metallic ions. Water molecules also present in between the layers. The general chemical composition of a typical LDH is given as

$$M(II)_{1-x}\, M(III)_x(OH)_2(A^{n-})_{x/n} \times yH_2O \ldots\ldots\ldots (1)$$

Where M(II) is a divalent cation, M(III) and An- is an interlayer anion. In this study we are using a magnesium-aluminum hydroxycarbonate having a chemical formula of $Mg_6Al_2(OH)_{16}CO_3.4H_20$ also known as hydrotalcite. A typical layered LDH structure is shown in Fig 1.5.

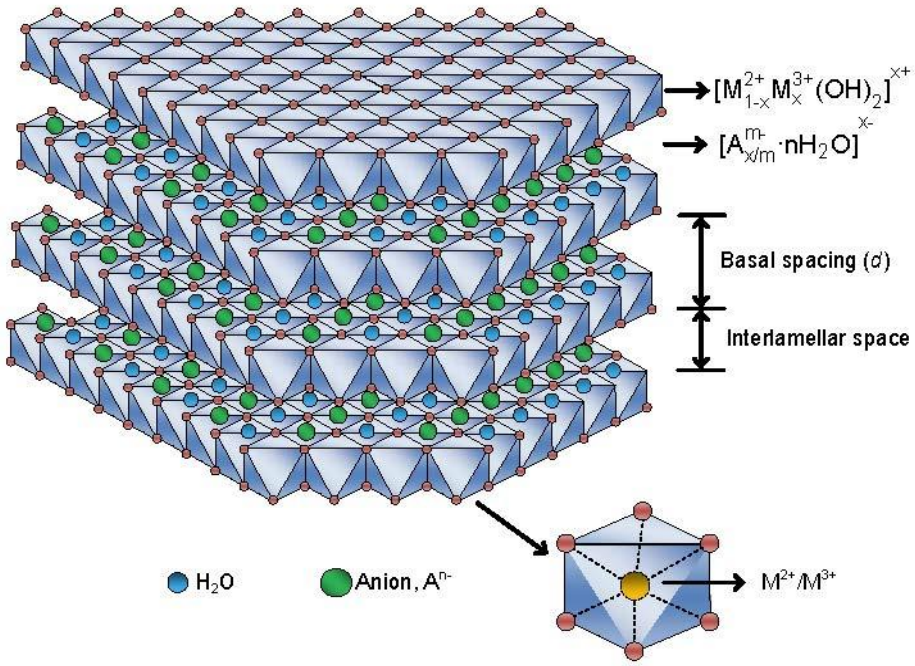

Figure 1. 5 Schematic of Layered Double Hydroxide [19]

Because of the large surface area and readily available active site for anion exchange between the metallic layers had enable the use LDH for various application such as water treatment [20], separation and capture of CO_2 from fuel gas [21], nuclear waste management [22] and biomedical applications. [23]

The positive charge of the metallic layers attracts the negatively charged biomolecules and pharmaceutical drugs which results in the intercalation of these within the metallic layer. LDH swell up to 20 A to accommodate the loading of drug or incoming biomolecule between the layers. The release of the drug is perform when the carboxylic acids or carboxylic derivatives, an anti-inflammatory agents present in the cardiovascular system interacts with the LDH. They undergo ion exchange with the anions intercalated within the layers, resulting in the control release of the drug. [24]

1.6 Scope of the Thesis

The objective of this thesis is to investigate the mechanical, thermal and electrochemical properties of a bioinspired coating having high filler percentage. Nanoparticles of Mg/Al carbonate, a layered double hydroxide (LDH) were added into biodegradable and biocompatible random copolymer Poly butyrate adipate terephthalate (PBAT) at 5, 15 and 50 % by wt.

Compressive and Dynamic mechanical analysis is used to observe the effect of higher filler concentration on the mechanical integrity of the nanocomposite. Also, the response of the polymeric chain incorporated with the LDH is observe under compressive and cyclic loading.

Nanoindentation is used to measure the elastic modulus and indentation hardness at the nano scale. Multi cyclic loading and unloading was performed to obtained the viscoelastic and viscoplastic properties of the composites. Plasticity Index is also calculated which relates to the intrinsic toughness of the material.

Differential Scanning Calorimeter (DSC) is used to measure the effect of LDH on the chain mobility during the thermal transition. Also, the effect of LDH as a nucleating agents on the crystallization temperature is examine using DSC cooling scans.

Scanning Electron Microscopy is use to observe the stacking of particle and the dispersion of nanoparticles in the matrix. The dispersion of the particles gives the higher surface area and also higher attachment site for potential drug uptake.

Potentiodynamic polarization method is used to investigate the corrosion mechanism, it gives the corrosion potential and current because of the ionic flow which is used to measure the corrosion resistance property.

1.7 Reference

[1] Wegst, U. G. K., Bai, H., Saiz, E., Tomsia, A. P., & Ritchie, R. O. (2015). Bioinspired structural materials. Nat Mater, 14(1), 23-36. Retrieved from http://dx.doi.org/10.1038/nmat4089.

[2] Glimcher, M. J. Bone: Nature of the calcium phosphate crystals and cellular, structural, and physical chemical mechanisms in their formation. Rev. Mineral. Geochem. 64, 223–282 (2006).

[3] Fratzl, P., H. S. Gupta, E. P. Paschalis, and P. Roschger. 2004. Structure and mechanical quality of the collagen-mineral nano-composite in bone. J.Mater.Chem. 14 (14): 2115-23, http://dx.doi.org/10.1039/b402005g.

[4] Barthelat, F., Tang, H., Zavattieri, P. D., Li, C. -, & Espinosa, H. D. (2007). On the mechanics of mother-of-pearl: A key feature in the material hierarchical structure. Journal of the Mechanics and Physics of Solids, 55(2), 306-337. doi:http://dx.doi.org/10.1016/j.jmps.2006.07.007

[5] http://sylvaindeville.net/

[6] Bose, S., Tarafder, S., & Bandyopadhyay, A. (2015). 7 - hydroxyapatite coatings for metallic implants. In M. Mucalo (Ed.), Hydroxyapatite (hap) for biomedical applications (pp. 143-157) Woodhead Publishing. doi:http://dx.doi.org/10.1016/B978-1-78242-033-0.00007-9

[7] Irena, Gotman. December 1997. Characteristics of Metals Used in Implants. Journal of Endourology., 11(6): 383-389. doi:10.1089/end.1997.11.383.

[8] Shahlari, Mahin and Lee, Sunggyu, "Biodegradable polymer /clay nanocomposites based on poly(butylene adipate-co-terephthalate) and poly(lactic acid)" (2008). Faculty Research & Creative Works. Paper 8962.

[9] Fukushima, K., Rasyida, A., & Yang, M. (2013). Characterization, degradation and biocompatibility of PBAT based nanocomposites. Applied Clay Science, 80–81, 291-298. doi:http://dx.doi.org/10.1016/j.clay.2013.04.015

[10] By Frank C. Müller (Own work) [CC BY-SA 2.5 (http://creativecommons.org/licenses/by-sa/2.5)], via Wikimedia Commons

[11] http://surgicalwatch.com/knee-replacements/

[12] http://surgicalwatch.com/hip-replacements/revision-surgery/

[13] http://ptvhc.com/u-s-fda-grants-expanded-labeling-claim-to-on-x-life-technologies-reducing-blood-thinning-requirements-for-heart-valve-patients/

[14] Vroman, I., & Tighzert, L. (2009). Biodegradable polymers. Materials, 2(2), 307. doi:10.3390/ma2020307

[15] Chen, Yiwang AND Tan, Licheng AND Chen, Lie AND Yang, Yan AND Wang,Xiaofeng. (2008). Study on biodegradable aromatic/aliphatic copolyesters. Brazilian Journal of Chemical Engineering}, 25, 321. Retrieved from http://www.scielo.br/scielo.php?script=sci_arttext&pid=S0104-66322008000200011&nrm=iso

[16] Rychter, P., Kawalec, M., Sobota, M., Kurcok, P., & Kowalczuk, M. (2010). Study of aliphatic-aromatic copolyester degradation in sandy soil and its ecotoxicological impact. Biomacromolecules, 11(4), 839-847. doi:10.1021/bm901331t

[17] Shahlari, Mahin and Lee, Sunggyu, "Biodegradable polymer /clay nanocomposites based on poly(butylene adipate-co-terephthalate) and poly(lactic acid)" (2008). Faculty Research & Creative Works. Paper 8962.

[18] Fukushima, K., Rasyida, A., & Yang, M. (2013). Characterization, degradation and biocompatibility of PBAT based nanocomposites. Applied Clay Science, 80–81, 291-298. doi:http://dx.doi.org/10.1016/j.clay.2013.04.015

[19] Conducting Polymers / Layered Double Hydroxides Intercalated Nanocomposites By Jairo Tronto, Ana Cláudia Bordonal, Zeki Naal and João Barros Valim DOI: 10.5772/54803.

[20] Kim JH, Park JA, Kim SB. (2012) Mg/Al layered double hydroxide for bacteriophage removal in aqueous solution. Water Sci Technol. 2012;66(4):761-7. doi: 10.2166/wst.2012.239.

[21] Wang, J., Stevens, L. A., Drage, T. C., & Wood, J. (2012). Preparation and CO2 adsorption of amine modified Mg–Al LDH via exfoliation route. Chemical Engineering Science, 68(1), 424-431. doi:http://dx.doi.org/10.1016/j.ces.2011.09.052

[22] Zümreoglu-Karan, B., & Ay, A. (2012). Layered double hydroxides-multifunctional nanomaterials. Chemical Papers, 66(1), 1-10. doi:10.2478/s11696-011-0100-8

[23] Kuthati, Y., Kankala, R. K., & Lee, C. (2015). Layered double hydroxide nanoparticles for biomedical applications: Current status and recent prospects. Applied Clay Science, 112–113, 100-116. doi:http://dx.doi.org/10.1016/j.clay.2015.04.018.

[24] P. Nalawade, B. Aware, V. J. Kadam, R. S. Hirlekar, J. Sci. Ind. Res. (India) 68, 267 (2009)

CHAPTER 2

LITERATURE REVIEW

2.1 Introduction

The macroscopic physical and mechanical properties of a composite material depend on the percentage of their constituents, their microstructure [1] and orientation in the matrix [2]. Biological materials have always been the source of inspiration, because of their ability to evolve, which had not only helped them to survive but also results in materials having exceptional mechanical properties and biological functionalities [3]. Materials such as bone and nacre are being widely studied, because of their complex hierarchical structure and the arrangement of minerals which provide superior toughness and strength, while still being lightweight [4,5,6].

The structure of human bone is composed of 10-20% collagen, 60-70% bone mineral, and 9-20% water by weight [7]. Collagen fibers having diameter from 100 to 2000 nm forms the structured matrix, which provide flexibility and tensile strength while the bone minerals are mainly hydroxyapatite crystals, which have plate or needle like shape in nanometer dimensions that reinforced the collagen fiber matrix leading to enhanced compressive strength and stiffness [8,7].

The mechanism of enhanced fracture toughness in bone and nacre is associated with the ability of the plates to move in response to mechanical stress. Since work of deformation is a product of force and displacement, the net displacements are associated with increased energy for fracture in bone and nacre. Hence, mimicking the biological structure is a reasonable approach that takes the field of polymer nanocomposites into a new realm. [9,10,11]. In polymer nanocomposites, a polymer

matrix is modified with small fractions of fillers. The filler in a nanocomposite is defined as one where at least one dimension is in the nano-scale. Thus nano-tubes, nano-spheres and nano-plates are all viable. In the case of the nature inspired architecture of bone as well as nacre, the ceramic constituent is of a platelet geometry. Thus in this paper we utilize the nano-platelets based in layer double hydroxides (LDH). LDH are anion exchanged clays also known as hydrotalcite, having a general formula $[MII_{1-x}MIII_x(OH)_{2x}]x+(An-)x/n.mH_2O$, where MII represents a divalent metal, MIII a trivalent metal, and An- an anion. They have a brucite-like structure in which a fraction of the divalent metal is replaced with a trivalent metal. The replacement gives the layers a positive charge, and anions are intercalated between these layers to maintain the electro neutrality.[12,13] Intercalation of organic compounds into LDHs provides a useful synthetic route to prepare organic-inorganic hybrids that contain properties of both the organic guest and the inorganic host in a single material.[14] The resulting properties can be tailored to a specific requirement needed to serve specific purposes. Extensive potential is being witnessed in the fabrication of bio based polymeric matrix with reinforcement of functional nanofillers such as layered double hydroxides (LDH), hydroxyapatite (HAp), cellulose nanofibers and silica nanoparticles because of the diversified functionalities they bring to the composites. [15,16,17]. For example, LDHs is being used for the controlled release of drugs and biomolecules [18,19,20,21], and silica nanoparticles for the improvement in thermal properties of polymer composites [22].

In this effort we utilize poly(butylene adipate-co-terephthalate) (PBAT) as the organic constituent. PBAT is an aliphatic aromatic polyester with excellent thermal, mechanical properties and biodegradability. Among its notable characteristics is a high

ductility that we hypothesize will function well to enable the platelet mobility. Research done by Kikku Fukushima et al [23,24] signifies the potential of using PBAT with different types of clay in biomedical applications.

CHAPTER 3

MATERIALS AND METHODS

3.1 Materials

3.1.1 Polybutyrate adipate terephthalate (PBAT)

A biopolymer PBAT having a commercial name Ecoflex® F BX 7011 was used as a matrix material for the composite coatings. It is a biodegradable aliphatic-aromatic co-polyesters having a molecular weight of 40,000 g/mol and density of 1.25 g/cm^3. It was provided BASF, Germany in granulate form.

3.1.2 Hydrotalcite: Aluminum Magnesium hydroxyl-carbonate (LDH)

Hydrotalcite is a layered double Hydroxide of Magnesium and Aluminum Metal. In which layers of aluminum and magnesium are joined by the carbonate and water molecules. The chemical formula for hydrotalcite is $Mg_6Al_2CO_3(OH)$ 4(H_2O). It comes with a commercial name of PURAL® MG 63 HT supplied by Sasol, Germany. The percentage of MgO:Al_2O_3 is 62-64:38-36. The particle size ranges between 3 and 9 µm, were as the crystallite size of the LDH was around 100 nm.

3.1.3 Phosphate Buffered Saline (PBS)

Dry powder of PBS was brought from Sigma Aldrich, it was dissolved in deionized water to yield 0.01 M of Phosphate buffered saline, 0.138 M of NaCl and 0.0027 M of KCl. The solution has a pH of 7.4 at 25 degrees C. It was use to stimulate the ionic concentration of body fluids. It was used as a solvent to perform corrosion experiments.

3.1.4 Chloroform

Chloroform containing amylenes as stabilizer, ACS reagent with 99.8% purity was purchased from Sigma Aldrich (USA) that was used for the preparation of solution of PBAT and respective percentages of LDH with PBAT for air spray application.

3.2 Nanocomposite Preparation

Nanocomposites containing 5%, 15% and 50% LDH with pure PBAT by weight percentage was prepared by melt mixing. Melt mixing is a process in which the nanoparticles are mixed with polymer at a temperature above the softening point of the polymer either statically or under shear. [25]. Prior to melt mixing the Hydrotalcite (LDH) was dried at 110^{o}C for 24 h to remove the moisture. The components were physically premixed in order to achieve better dispersion of nanoparticles in the polymer, before being fed to the two piece mixer with banbury blades in Brabender® CWB model D-52, having a capacity of 40 gm. Melt blending was performed at 160^{o}C with 50 rpm for 8 min. Torque and melt temperature was continuously monitored. The mixture was air cooled and subsequently cut into pellet-sized pieces using a Fritsch pelletizer.

3.3 Sample Preparation

3.3.1 Compression Test

Circular disc were prepared for the compression test having a diameter of 25mm and a thickness of 2mm. Circular Aluminum mold was filled with the pellets, and then placed in a Carver Lab hot press model: 3925, pressed with a force of 30,000 pound at 160 °C for 10 minutes, in between breathing (pressure was release and then reapplied) was done thrice in order to remove bubbles and have a homogenous sample. The samples were cooled maintaining the applied force through water circulation to room temperature.

3.3.2 Dynamic Mechanical Analysis

Rectangular mold was used to made samples having length of 25 mm, width of 12.5 mm and a thickness of 2mm. Samples were prepared using the same process as used for compression test samples.

3.3.3 Nanoindentation Test

Carver Lab hot press model: 3925 was used to made nanoindentation sample of pure PBAT along with 5%, 15% and 50% by wt. LDH-PBAT nanocomposites coating, a uniform film having thickness of 1 mm was prepared on the steel substrate by compression molding.

3.3.4 Differential Scanning Calorimeter (DSC)

The pellet-sized pieces of pure PBAT and 5%, 15% and 50% LDH-PBAT nanocomposites from the Fritsch pelletizer were enclosed in 50 µL aluminum pan. The samples were weight in between 5 to15 mg. The thermal properties of the nanocomposites were compared with an empty 50 µL aluminum pan taken as base for the differential Scanning Calorimeter.

3.3.5 Electrochemical Test

Low carbon steel samples having dimension (25x25x3mm) were used for the biomimetic coating application. The low carbon steel samples surface were ground with 120, 400 and 800 grade SiC papers before the application of the coating with an air spray. The solution of PBAT, 5%, 15% and 50% of LDH-PBAT was prepared by dissolving 10% by wt. the polymer in chloroform solvent and then adding respective amount of LDH in the solution for air spray application.

3.4 Methods

3.4.1 Compression Test

Typically the tensile strength of a cortical bone in longitudinal direction is 60-70 MPa while in transverse direction around 50 MPa. Moreover the compressive strength of bone ranges from 70 MPa to 280 MPa in longitudinal direction while 50 MPa in the transverse direction [26]. The compressive mechanical properties of nanocomposites were investigated to observe the effect of LDH particle on a polymer which has low load bearing capability.

Measurements of compressive mechanical properties of the prepared nanocomposites were performed on a hydraulic MTS machine under room temperature. Hot press was used to make circular shape samples having a cross-sectional area of 40 mm^2 and a thickness of 2.0 mm. The crosshead speed of 0.1 mm/min was used to perform the compression tests as indicated by Vidhate et al. [27]. Young modulus was determined by the elastic region of the stress strain curve while compressive yield strength was calculated by the amount of load applied at yield point divided by the initial cross-sectional area.

3.4.2 Dynamic Mechanical Analysis

To measure the glass transition temperature and the effect of addition of LDH on the elastic and viscous response of the blend, dynamic mechanical analysis (DMA) was perform using dynamic mechanical analyzer RSA III (TA Instruments, New Castle, DE). The samples were tested in bending mode. The samples were scanned from minus 50^{o}C to 5^{o}C at a heating rate of 5^{o}C per min, at frequency of 1 Hz. To avoid the plastic deformation of the sample a strain amplitude of 0.2% was set, which was determine by strain amplitude sweep test at 1 Hz on a separate sample.

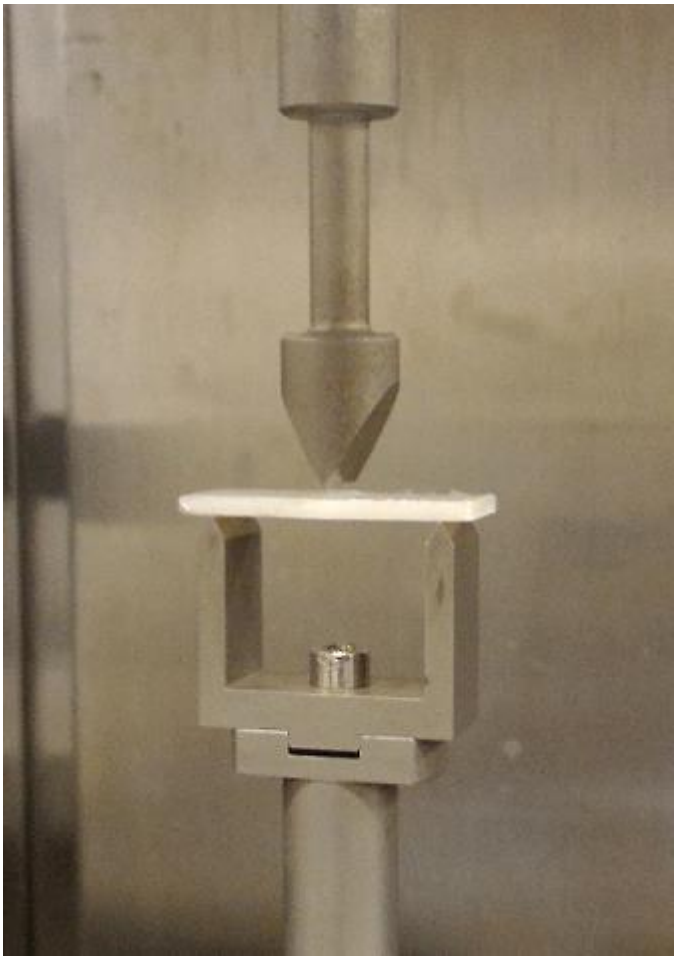

Figure 3. 1 Dynamic Mechanical Testing in three point bending mode.

3.4.3 Nanoindentation Test

The MTS nanoindenter XP was used following a Continuous Stiffness Method (CSM) Standard Hardness/Modulus with a diamond Berkovich tip having an elastic modulus of 1141 GPa and a Poisson ratio of 0.07[28]. To cancel out the effect of environment a combination of a minus k vibration isolation table and a thermal vibration isolation cabinet was used. Prior to the testing, the nanoindentaion system was tested for calibration on fused silica sample. Each of the sample were indented to 2000 nm, while the allowable drift rate was set to 0.05 nm/s with a maximum thermal drift time of 3 h. Poisson ratio of PBAT was taken 0.49 as mention by Roche et al[29], same value was assumed for all the nanocomposite samples while calculating the elastic modulus.

The values of Modulus and Hardness were calculated assuming material to be isotropic as mentioned by Oliver and G.M Pharr [30,31]. Modulus of the film E_S was calculated by equation 2.

$$\frac{1}{E_r} = \frac{1-\vartheta_s^2}{E_s} + \frac{1-\vartheta_i^2}{E_i} \dots\dots\dots\dots (2)$$

Er = Reduce Modulus, Es = Modulus of fiber, Ei = Indenter Modulus, Vs = Poisson ratio of fiber, Vi= Poisson ratio of indenter, whereas Er is given by

$$E_r = \frac{\sqrt{\pi}}{2}\frac{S}{\sqrt{A_c}} \dots\dots\dots\dots (3)$$

$S = contact\ Stiffness$, $A_c = contact\ area$

While the hardness is given by

$$H = \frac{P}{A_C} \ldots\ldots\ldots\ldots (4)$$

Where P= Load and Ac is the contact area.

Plasticity Index (Ψ) is the material property which identify the amount of plastic and elastic deformation occurs in the material once it is subjected to load. In nano-indentation it can calculated by measuring the ratio of irreversible energy stored due to plastic deformation to the total deformation energy (due to plastic and elastic deformation) during loading and unloading cycle. Figure 3.2 shows a typical nanoindentation loading and unloading cycle for a viscoelastic-plastic material. A_1 is the area between loading and unloading curve, quantify the amount of energy dissipated due to irreversible plastic deformation. While A_2 is the area under the unloading curves quantifying the reversible viscoelastic deformation. Plasticity Index is calculated using equation 5 as done by Patel et al for poly (para-phenylene vinylene) polymer films [32]. For the material to be completely elastic energy dissipated due to plastic deformation should be zero $(A_1 = 0)$ giving plasticity index $\Psi = 0$. Similarly for pure plastic deformation the $\Psi = 1$, for $0 < \Psi < 1$ the material is viscoelastic plastic.

$$\Psi = \frac{A_1}{A_1 + A_2} \ldots\ldots\ldots\ldots (5)$$

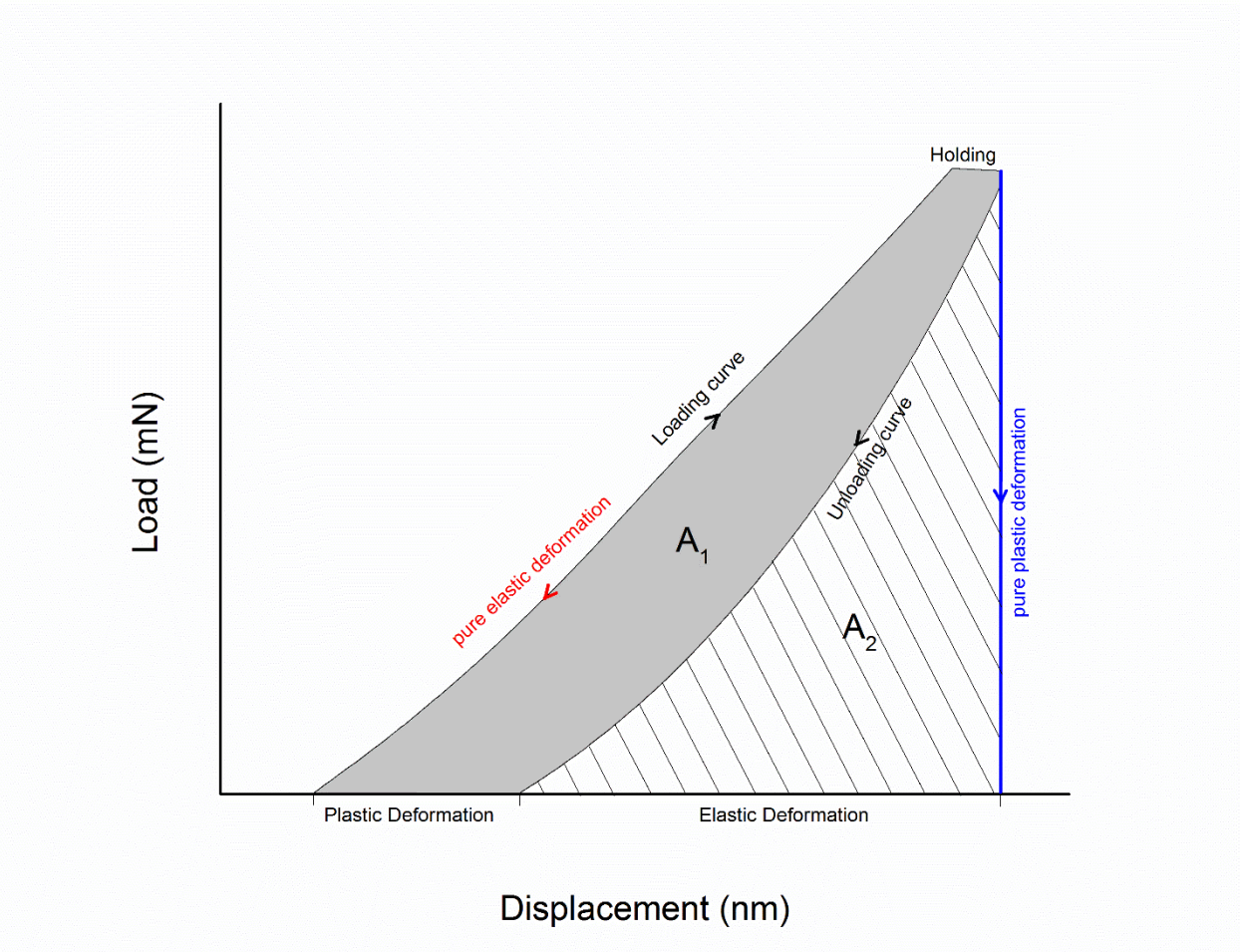

Figure 3. 2 A typical Nanoindentation load-displacement curve of a viscoelastic-plastic material.

MTS nanoindenter XP was also used to do a cyclic incremental loading test on pure PBAT with all of its blends to measure the viscoelasticity of the coatings. This type of incremental cyclic loading and unloading is normally performed to observe the phase transformation [33], micro cracks propagations [34] and to study the viscoelastic properties of the material[35,36] The load dependent indentation was applied at the same spot using the standard MTS nanoindenter XP cyclic loading test to observe the response of different percentage of clay in the polymer matrix. In seven cycles an

incremental indentation load was applied at 0.97, 1.95, 3.90, 7.81, 15.6, 31.3 and 62.5 mN. The peak load was hold for 5 sec at each cycle while the loading time was set to 10 sec to unload to the 10% of the applied load to measure the viscoelastic recovery in each cycle.

To measure the viscoelasticity of the nanocomposites coating each sample was indented to a fixed load and then relaxed to the 10% of the applied load to maintain the contact of the tip to the material. In the next cycle it was incremented to the higher load resulted in the generation of a hysteresis loop which gives the measure of viscoelasticity of the material as mentioned by Richter et al. [37]. Figure 3.3 shows the area of the loop which gives the absolute viscoelasticity (E_L) of the material which increases subsequently in successive cycles due to the incremental load. The absolute viscoelasticity was normalized by dividing with the ideal elastically stored energy (E_S) to get a relative viscoelastic energy which is uniform in all cycles.

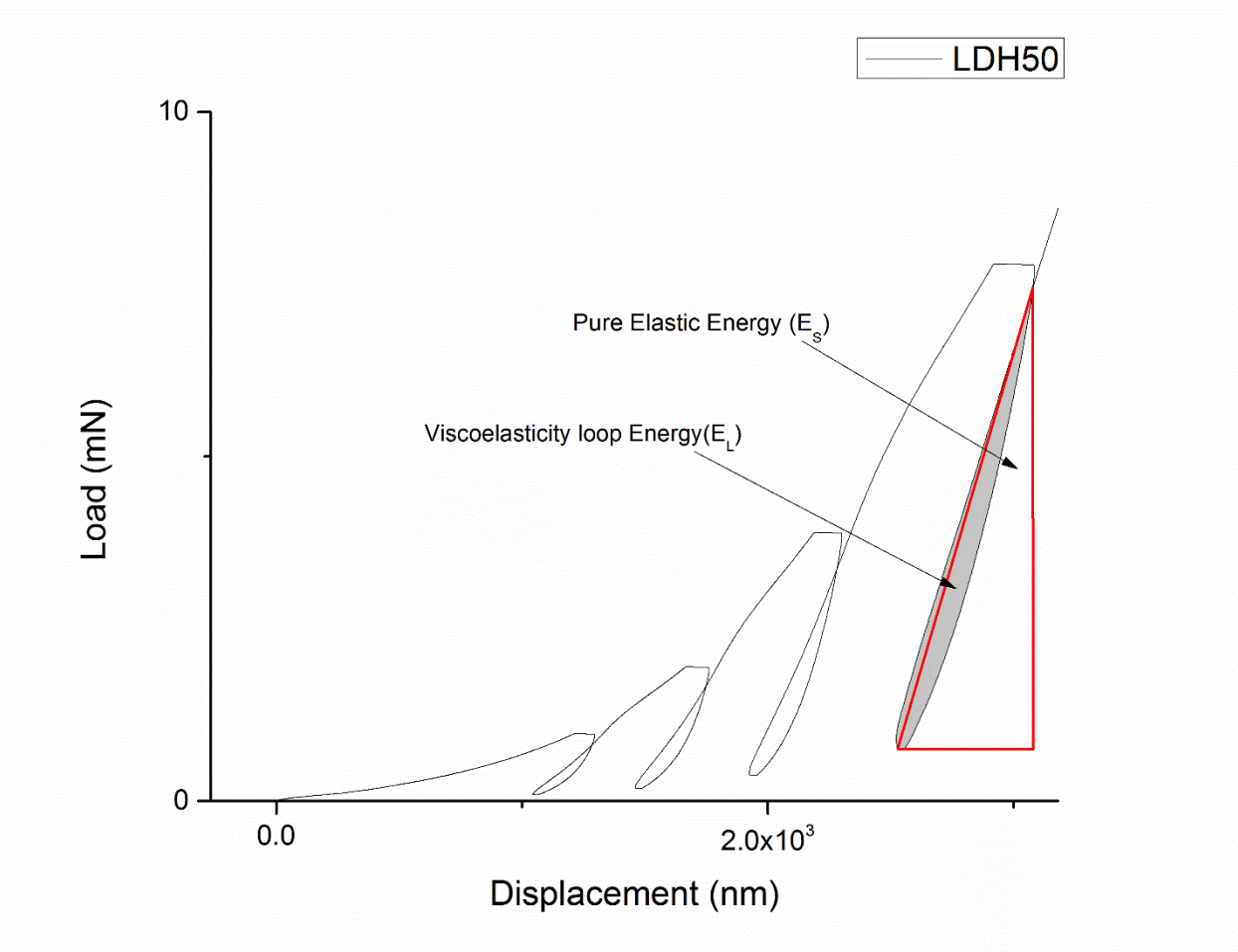

Figure 3. 3 Hysteresis Loop formation due to cyclic loading of LDH50 nanocomposite

3.4.4 Differential Scanning Calorimeter (DSC)

A Perkin Elmer DSC6 differential scanning calorimeter, equipped with a Perkin-Elmer Chiller was used for thermal analysis. The samples were placed in a nonvolatile aluminum pan weighing between 8 and 10 mg. The samples were held at 30°C for 2 minutes and then heated at the rate of 10^{o}C per minute from 30°C to 200°C. They were maintained at 200°C for 2 minutes and cool down from 200°C to 30°C at the same rate. This was the first heating and cooling cycle, the profile was repeated for the second

heating and cooling cycle. The enthalpy of fusion was calculated from the heating scans, while enthalpy of crystallization was calculated from the cooling scans.

3.4.5 Electrochemical Test

Corrosion is one of the major shortcoming of metallic implants. It occurs because of the incompatibility of implant with the ionic nature of the fluid in contact. Metallic corrosion mainly occurs due to the electrochemical reactions at the interface between the metal and the electrolyte solution. This results in the corrosion or encapsulation of the implant by the fibrous tissue, effecting the functionality of the implant.

The rate of corrosion of metals depends upon the equilibrium of the anodic and cathodic reaction. The general form of anodic reaction is given as

$$M \rightarrow M^{n+} + ne^{-}$$

In which a metal is oxidize by releasing electrons, whereas as value of n varies with the metal being univalent or multivalent. Cathodic reaction occurs as the solution ionic species is reduced by taking the electron. The general reaction is given as

$$H^{n+} + ne^{-} \rightarrow H$$

When the cathodic and anodic reactions are in equilibrium, the net electron flow between the metal and the electrolytic fluid is zero. The potential of the metal at which the net flow of electrons is zero is called open circuit potential (E_{OC}). The value of the anodic or cathodic current at open circuit current is called correction current (I_{CORR}) which is used to measure the rate of corrosion of the material.

There is no direct measurement method for the corrosion to measure the corrosion current, however it can be estimated using electrochemical techniques. Potentiostatic polarization is used to measure the current by varying the voltage using a potentiostat. As the potential of the sample moves away from its open circuit voltage it polarize and gives either a cathodic or anodic current. In this measuring technique the potential is varied for a range of values having E_{OC} as the center point. Hence it captures both cathodic and anodic polarization. Figure 3.4 shows a typical potential verse logarithmic current graph that is generated as a result of potentiostatic polarization known as Tafel plot.

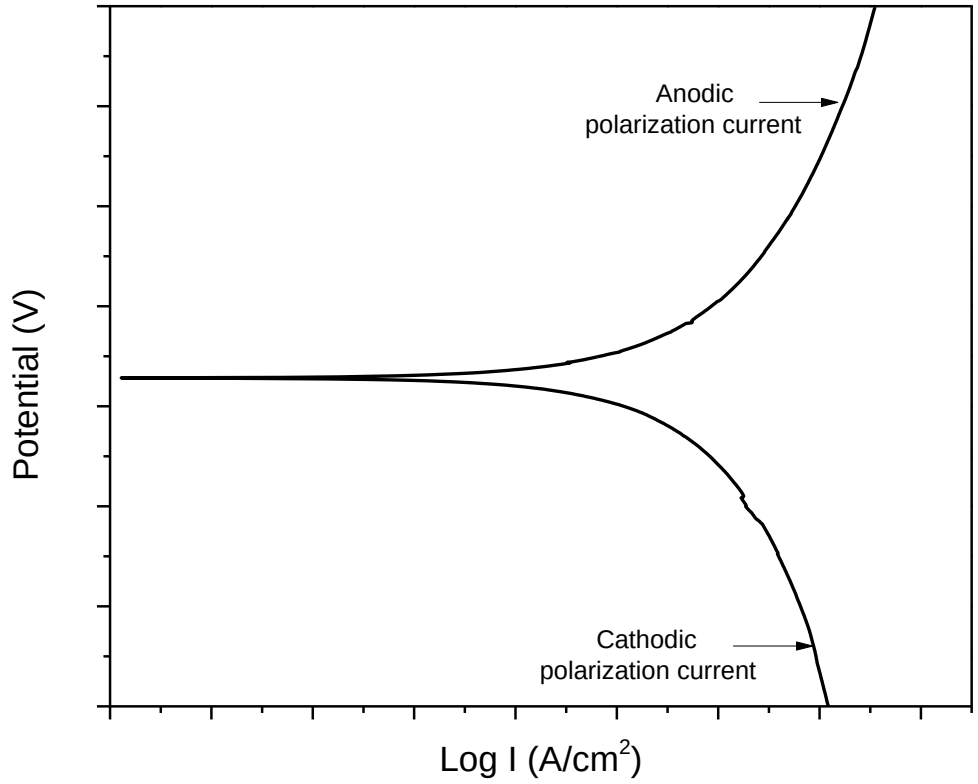

Figure 3. 4 A typical potential verses logarithmic current Tafel plot

Equation of each anodic and cathodic polarization curve knows as Tafel equation is given as

$$I = I_0 e^{\frac{2.303(E-E_0)}{\beta}} \ldots\ldots\ldots\ldots (6)$$

Where,

$I = the\ current\ generated\ from\ the\ reaction$

$I_0 = current\ at\ equilibrium\ (constant\ for\ a\ particular\ reaction)$

$E = Electrode\ potential$

$E_0 = equilibrium\ potential\ (constant\ for\ a\ particular\ reaction)$

$\beta = Tafel\ constant$

Equation 6 describe the phenomena of one reaction either anodic polarization or cathodic polarization. However in a corrosion system, there are two reactions occurring simultaneously. The metal is being reduce by giving up an electron, while the electrolyte is oxidize by taking up the electron. Hence for each of the reaction there is a tafel equation which is combined to give Butler-Volmer equation given as

$$I = I_{COOR}\left[e^{\frac{2.303(E-E_{COOR})}{\beta_a}} - e^{\frac{2.303(E-E_{COOR})}{\beta_b}}\right] \ldots\ldots\ldots\ldots (7)$$

Where,

$I_{COOR} = Corrosion\ current\ in\ Amperes$

$E_{COOR} = Corrosion\ potential\ in\ Volts$

$\beta_a = Anodic\ Tafel\ constant\ in\ volts/decades$

$\beta_c = Cathodic\ Tafel\ constant\ in\ volts/decades$

Fig 3.5 represent the estimation procedure to calculate the corrosion current from a typical Tafel plot. The linear region of the anodic and cathodic polarization curves are extrapolated linearly until they intersect at a point. The value of each of the anodic and cathodic current at this intersection point is called the corrosion current (I_{COOR}).

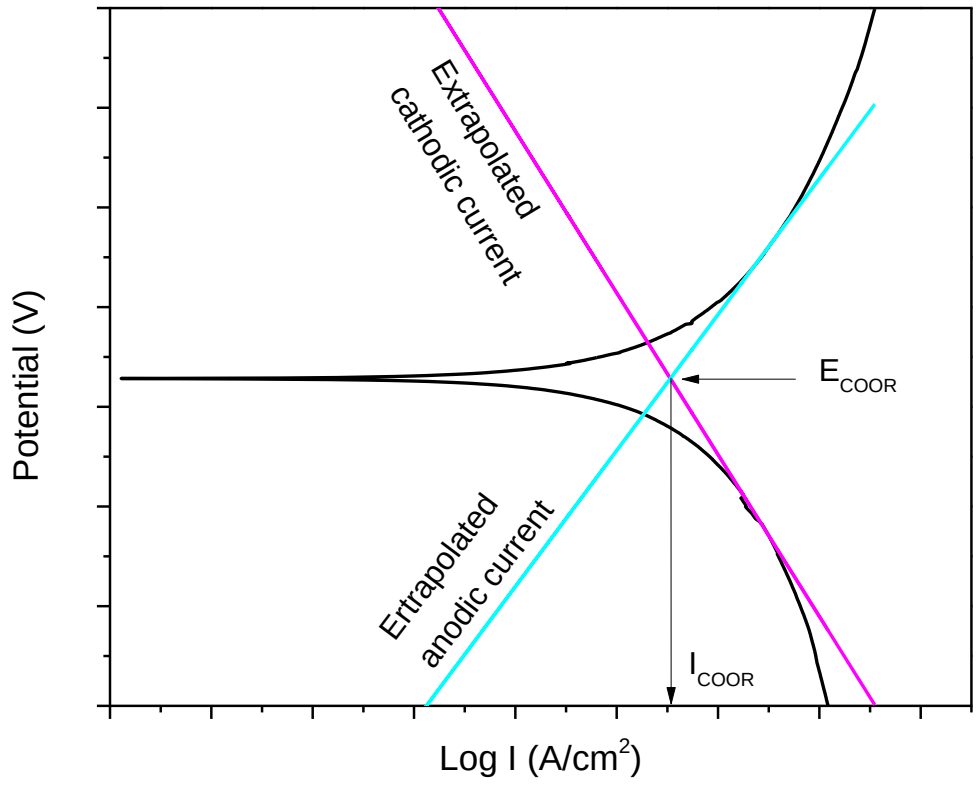

Figure 3. 5 Estimation of the corrosion current from Tafel plot.

Potentiodynamic polarization method was used to investigate the corrosion mechanism in Phosphate Buffer Saline (PBS) solution having pH of 7.4 to estimate the anodic and cathodic Tafel slopes. A Princeton/Applied Research (Parstat Model 2273)

was used to perform the electrochemical measurements. A three electrode flat cell utilizing Saturated Calomel Electrode (SCE) reference electrode was used for electrochemical measurements. The potential energy range E_o is (-1.0 V), E_1 (0.2 V) scan rate is 0.166 mV/s, and step height 0.5 mV, the exposed area in the electrode is (1cm2). Linear sweep resistance method was used to obtain the corrosion rate (CR).

3.4.5 Scanning Electron Microscope (SEM)

The morphology of the cross-section of prepared samples was examined in a SEM system (FEI Nova NanoSEM 230). The neat PBAT and different LDH percentage samples were coated to image the cross section at an accelerating voltage of 13 kV at a 5 mm working distance. The samples were sputter coated with gold-palladium to make them conductive and make imaging possible.

CHAPTER 4

RESULTS

4.1 Compression Test

Table 4.1 shows the increase in the young's modulus of the nanocomposites as the percentage of LDH increases. The modulus increased from 55.6 MPa for pure PBAT to 226.9 MPa for LDH50 nanocomposites i.e. about 400% increase. Figure 4.1 shows that the elastic region becomes steeper as the composite stiffness increases with the increase of LDH percentage. Compressive strength also increases which signifies the uniform dispersion of particles throughout the polymer matrix, as nanoparticles affectively plays the role of load bearing component in the matrix as well as provide the active site along the polymer matrix that enhanced the attachment of potential drug. Hence melt mixing and pressing the sample to stack the particles is an effective way for dispersion and layer formation of LDH in the polymer.

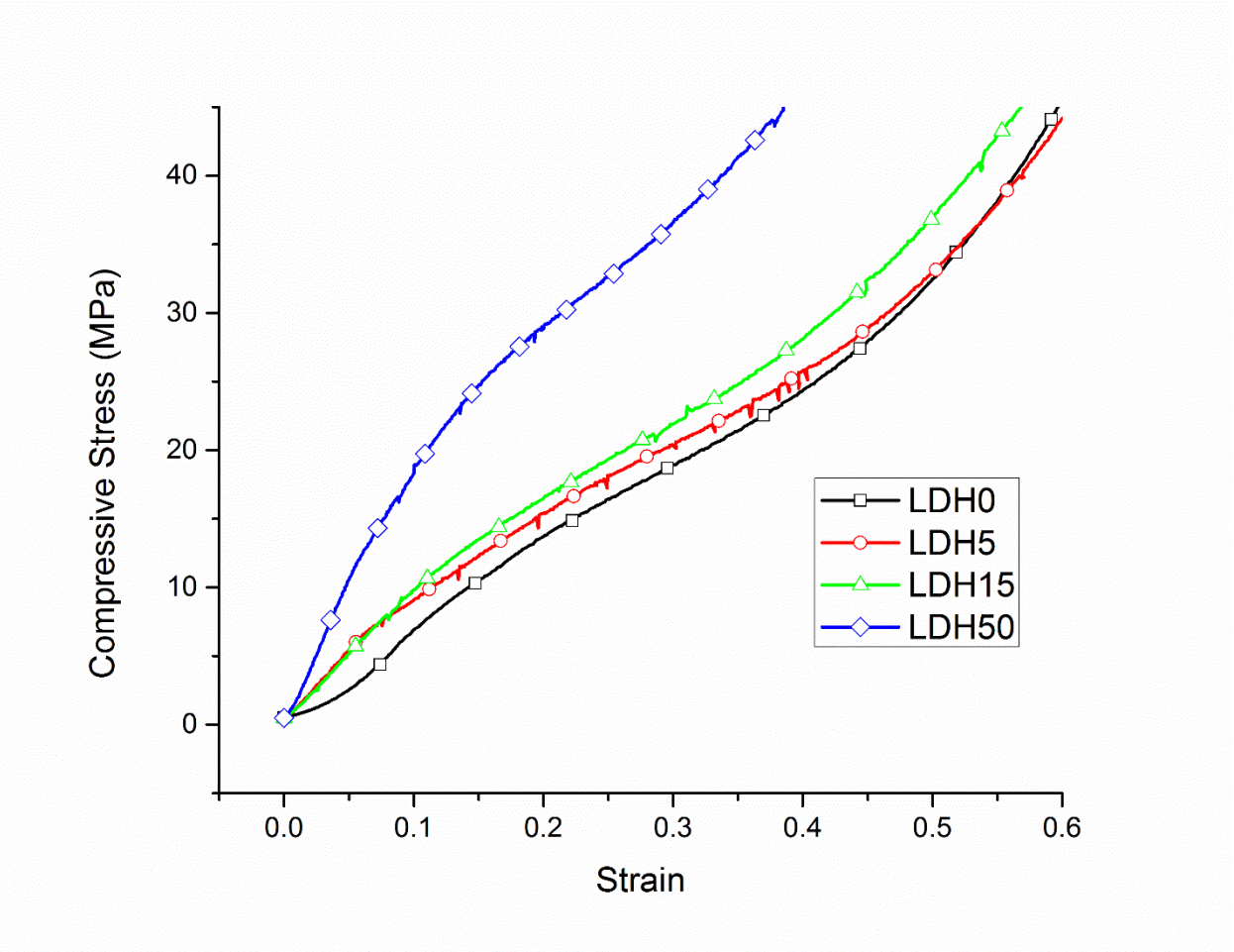

Figure 4. 1 Stress-Strain curve of LDH0, LDH5, LDH15 & LDH50 nanocomposite.

Table 4.1 Young's Modulus & Compressive Yield Strength of PBAT with different percentage of LDH.

Sample	**Young's Modulus (MPa)**	**Compressive Yield Strength (MPa)**
LDH0	55.6 ± 2.6	1.94 ± 0.2
LDH5	89.3 ± 10.0	9.03 ± 1.2
LDH15	108 ± 19.1	9.92 ± 2.2
LDH50	226.9 ± 11.2	24.9 ± 1.1

4.2 Dynamic Mechanical Analysis

The addition of the LDH resulted in enhanced glassy modulus and no significant change in the peak temperature of the loss modulus-temperature profile. Before the glass transition region at -45°C, we observed an increase of 88.8% for LDH50 nanocomposites as compared to neat PBAT. After the glass transition region at 0°C, the increase in glassy modulus was more than 400% for 50% LDH-PBAT as compared to neat PBAT. The glass transition values are all around -22 °C showing negligible change relative to the matrix. More significantly the peak of the loss modulus shows an increase with increasing LDH supporting the bio-inspired deformation at low oscillatory strain.

Table 4.2 Dynamic Mechanical Analysis of pure PBAT and all of its blends

Sample	Tg	Storage Modulus E' (MPa)			Loss Modulus (MPa)
	(^oC)	E'_{-45^o}	E'_{Tg}	E'_{5^o}	E''_{Tg}
LDH0	-22.4	609	150	74	35.8
LDH5	-22.8	622	151	77	36.3
LDH15	-23.0	722	197	95	42.1
LDH50	-23.6	1150	712	359	80.7

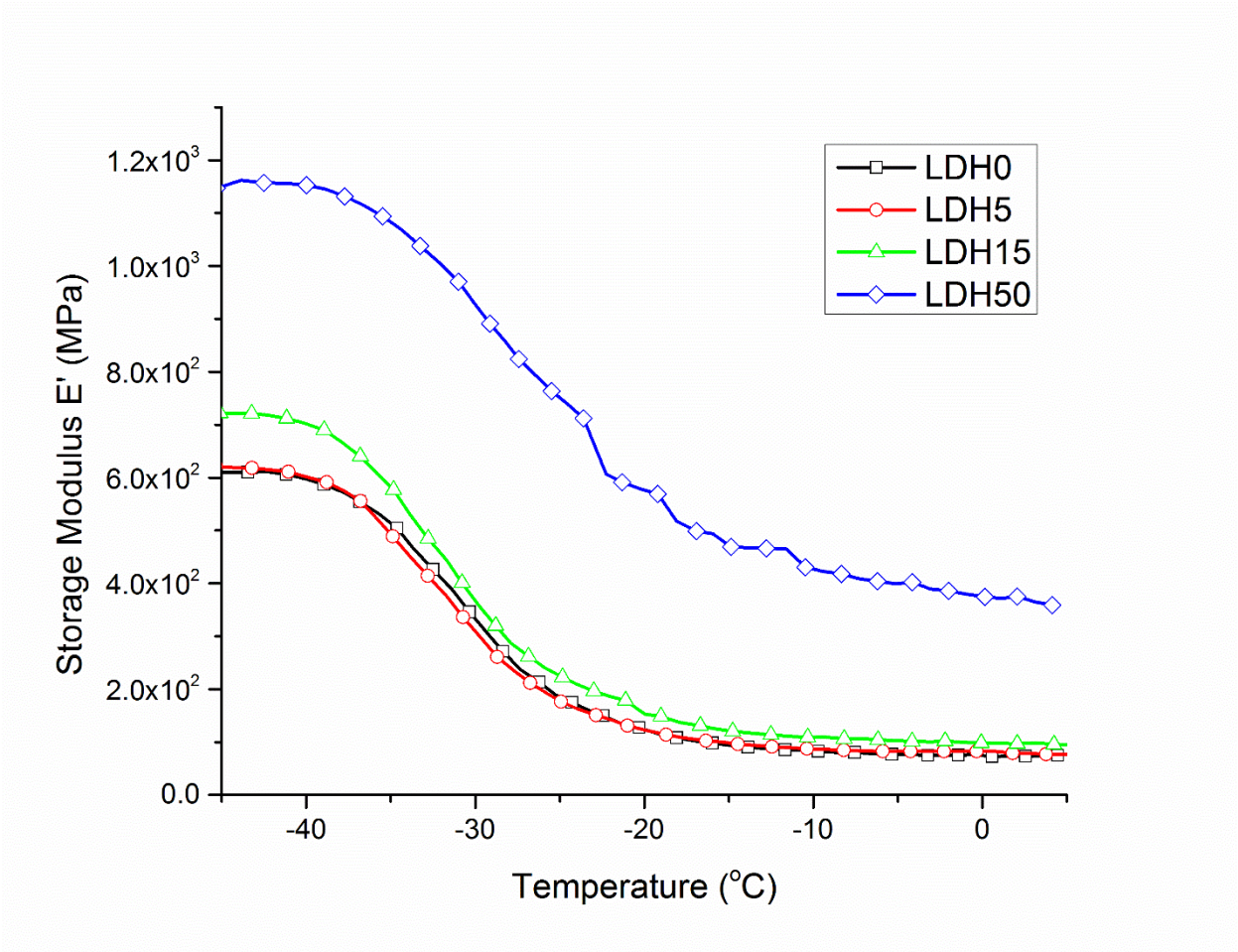

Figure 4. 2 Storage Modulus vs Temperature of PBAT and their blends.

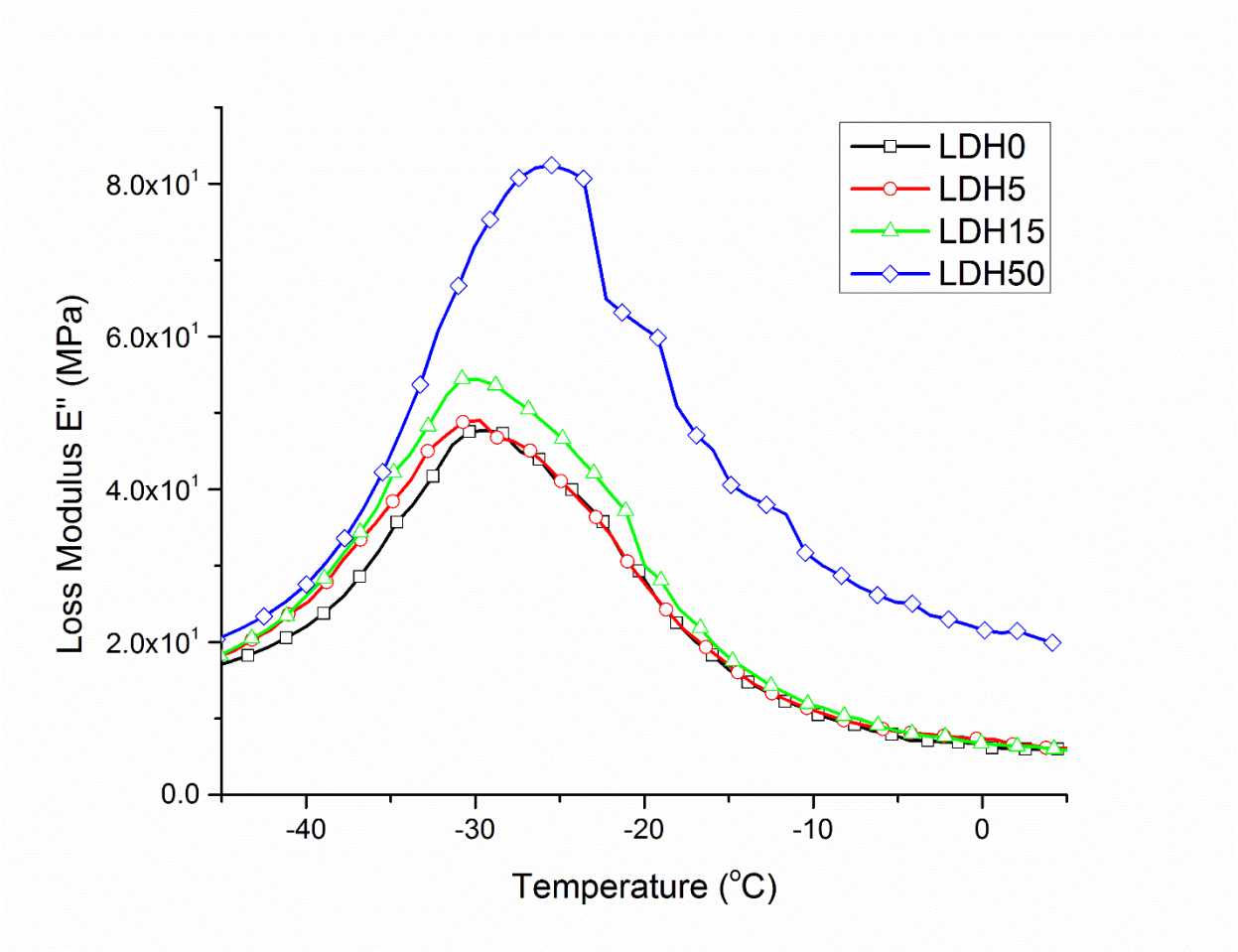

Figure 4. 3 Loss Modulus vs Temperature of PBAT and their blends.

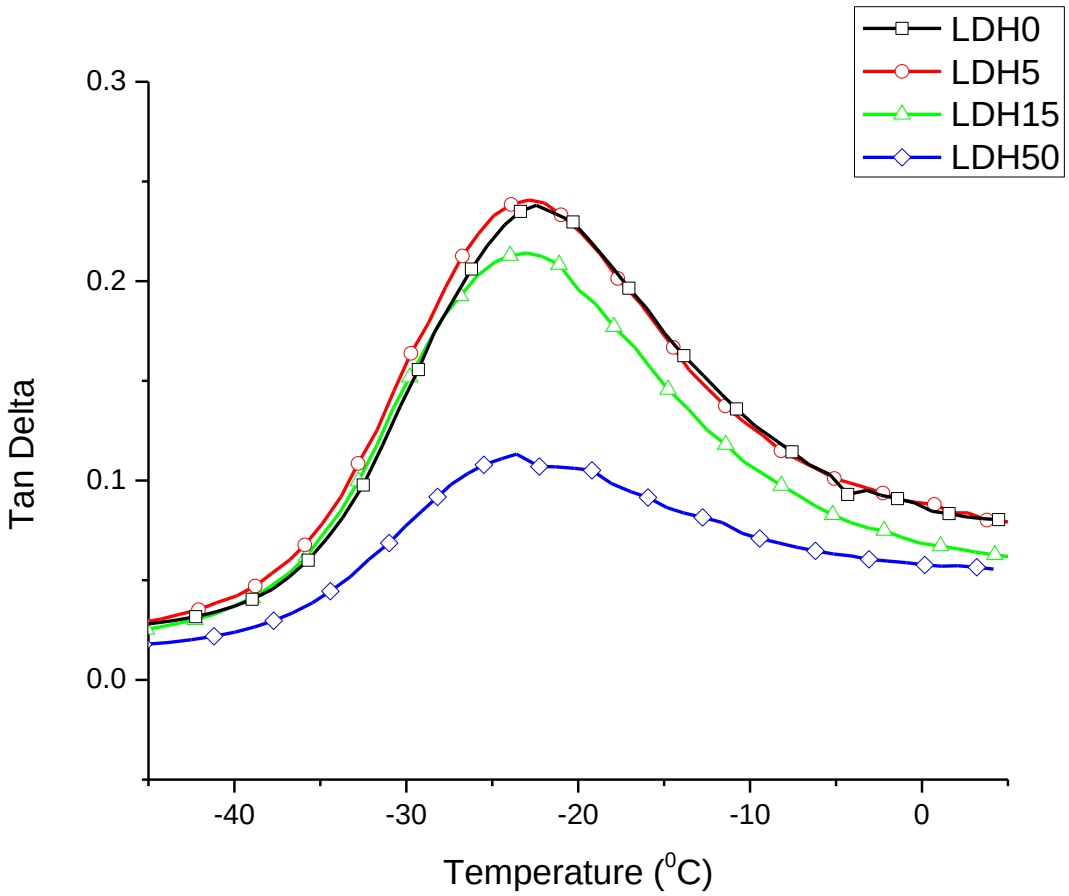

Figure 4. 4 Tan delta vs temperature of all PBAT and their blends.

4.3 Nano-Indentation

The hardness of the pure PBAT and different filler percentage of LDH was measured at a load of 1mN. Figure 4.5 shows a linear relation between the percentages of clay content with hardness value. Results were obtained using equation 3 as mentioned by Oliver and Pharr [30,31]. Table 4.3 shows the hardness and modulus values calculated by using equation 1 and 2 for pure PBAT, 5% LDH-PBAT, 15% LDH-PBAT and 50% LDH-PBAT for a single loading and unloading cycle. The results shows that the elastic modulus increased from 151 MPa for pure PBAT to 332 MPa for LDH50, which is more than 100% increase. Also the hardness of the composite also increases from 19.1 MPa for pure PBAT to 27.8 MPa to LDH50, almost a 45% increase. Hence LDH is successively enhancing the modulus and hardness of the coating.

Table 4.3 Modulus and Hardness calculated using single cycle Nano-indentation

Sample	**Modulus (MPa)**	**Hardness at 1mN (MPa)**
LDH0	151 $\pm$ 11.8	19.1 $\pm$ 2.54
LDH5	183 $\pm$ 8.9	21.2 $\pm$ 0.92
LDH15	206 $\pm$ 16.3	22.7 $\pm$ 0.63
LDH50	332 $\pm$ 81.2	27.8 $\pm$ 6.11

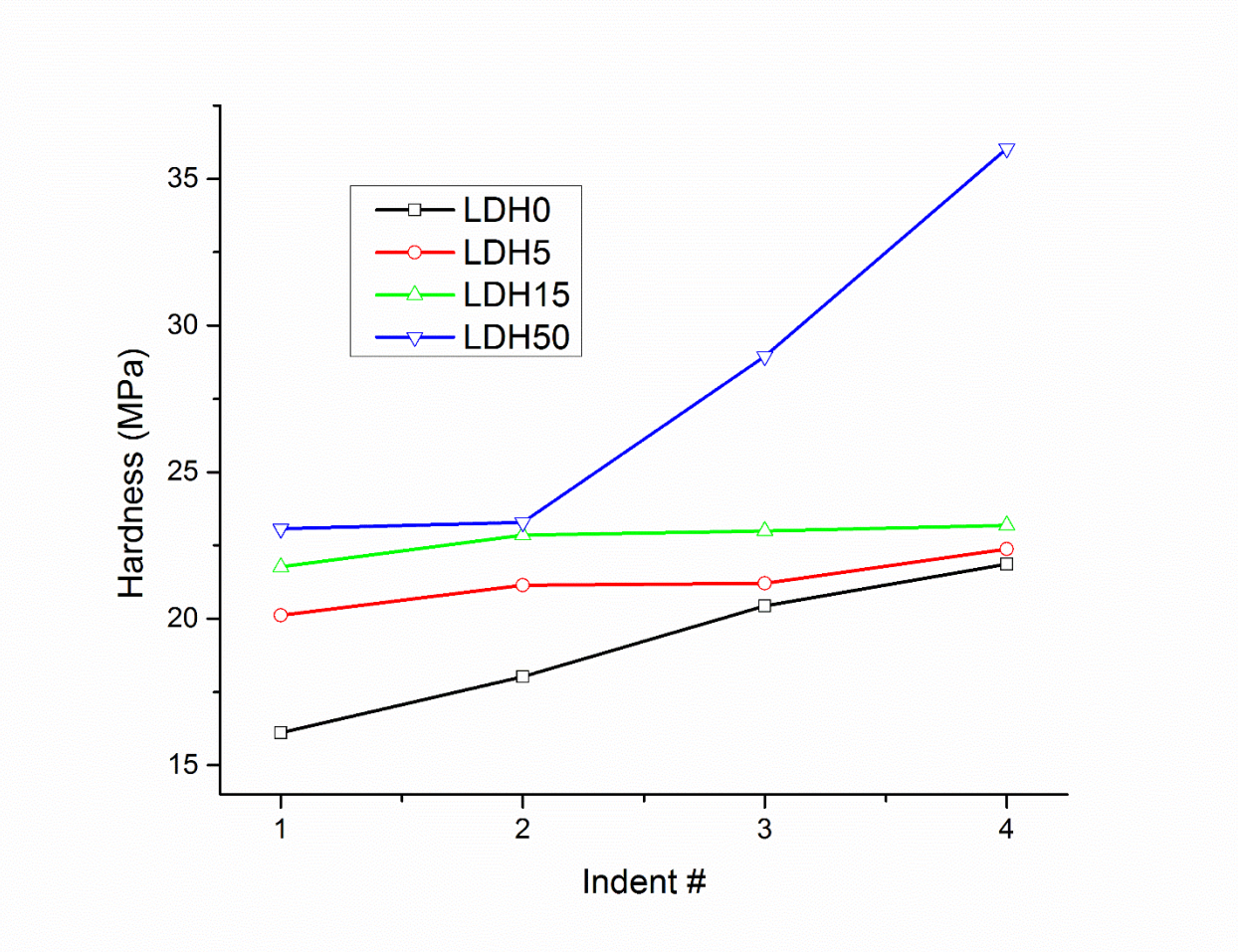

Figure 4. 5 Hardness of nanocomposites at 1mN.

Figure 4.6 shows the plasticity Index of the nanocomposites i.e. is the ratio of plastic deformation to the total deformation is increasing with the addition of LDH particles, which is a strange phenomenon as the hardness and modulus of the coating is also increasing. Maybe with the addition of the LDH, at Nano scale there is an increase in the defect sites within the nanocomposites which may cause an increase in the plasticity, as mention by youssaf et al. that addition of clay increases the plasticity and ion mobility in plastic crystal [38]. The increase in plasticity relates to the intrinsic

toughening mechanism which inhibits the initiation and propagation of cracks. Hence with the increase in the LDH percentage the composite becomes tougher [39].

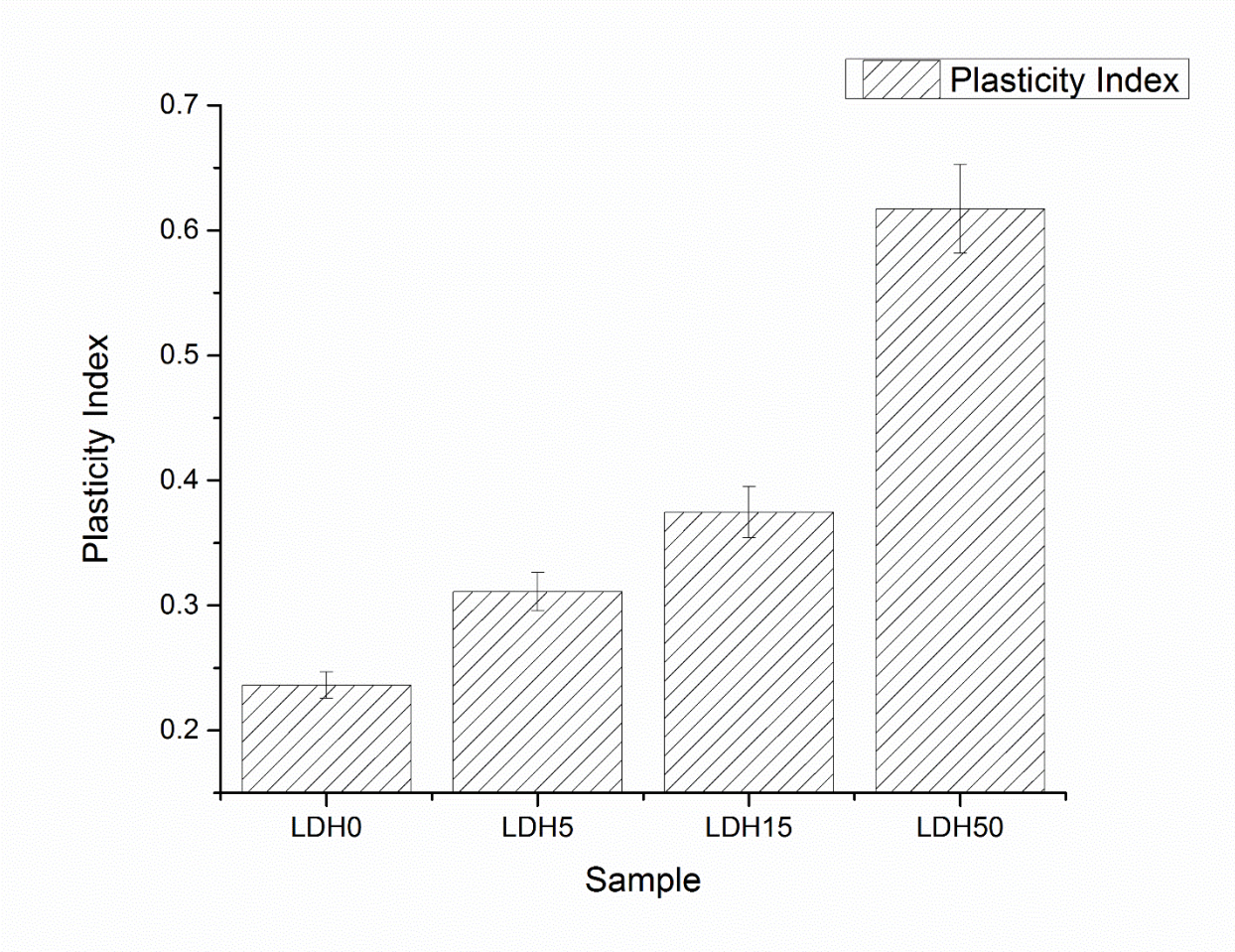

Figure 4. 6 Plasticity Index of LDH0, LDH5, LDH15 & LDH50 nanocomposites.

Figure 4.7 shows the load verses displacement graph of incremental cyclic loading applied to the samples at the same spot to observe the viscoelastic recovery of the composite. We can observed the composite goes to more of plastic deformation as the elastic deformation tends to decrease with the added concentration of clay. Moreover the stiffness, which is calculated by the slope of unloading curve increases with successive cycle and with the addition of LDH.

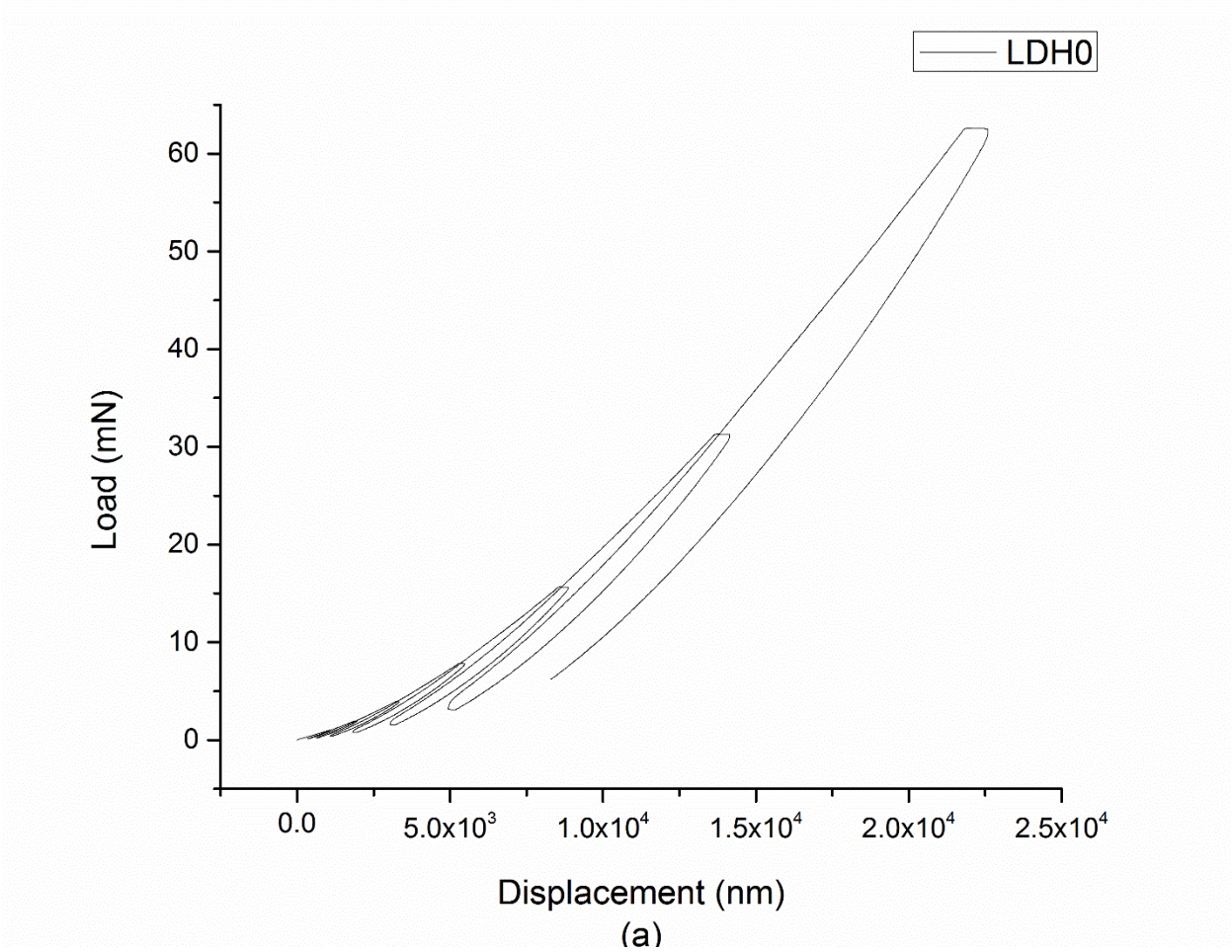

Figure 4. 7(1) Graphical Representation of seven cycle indentation of LDH0.

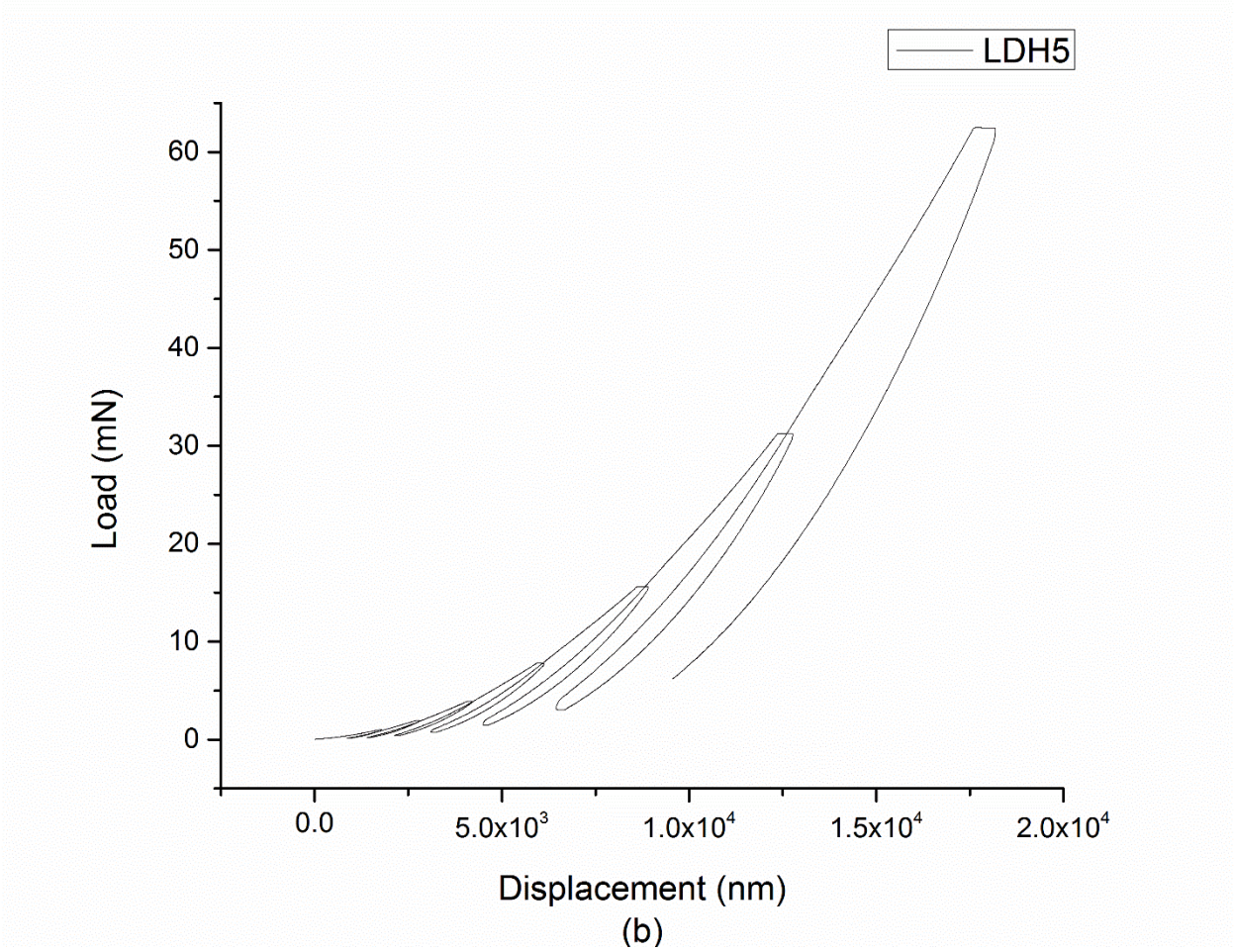

Figure 4. 7(2) Graphical Representation of seven cycle indentation of LDH5.

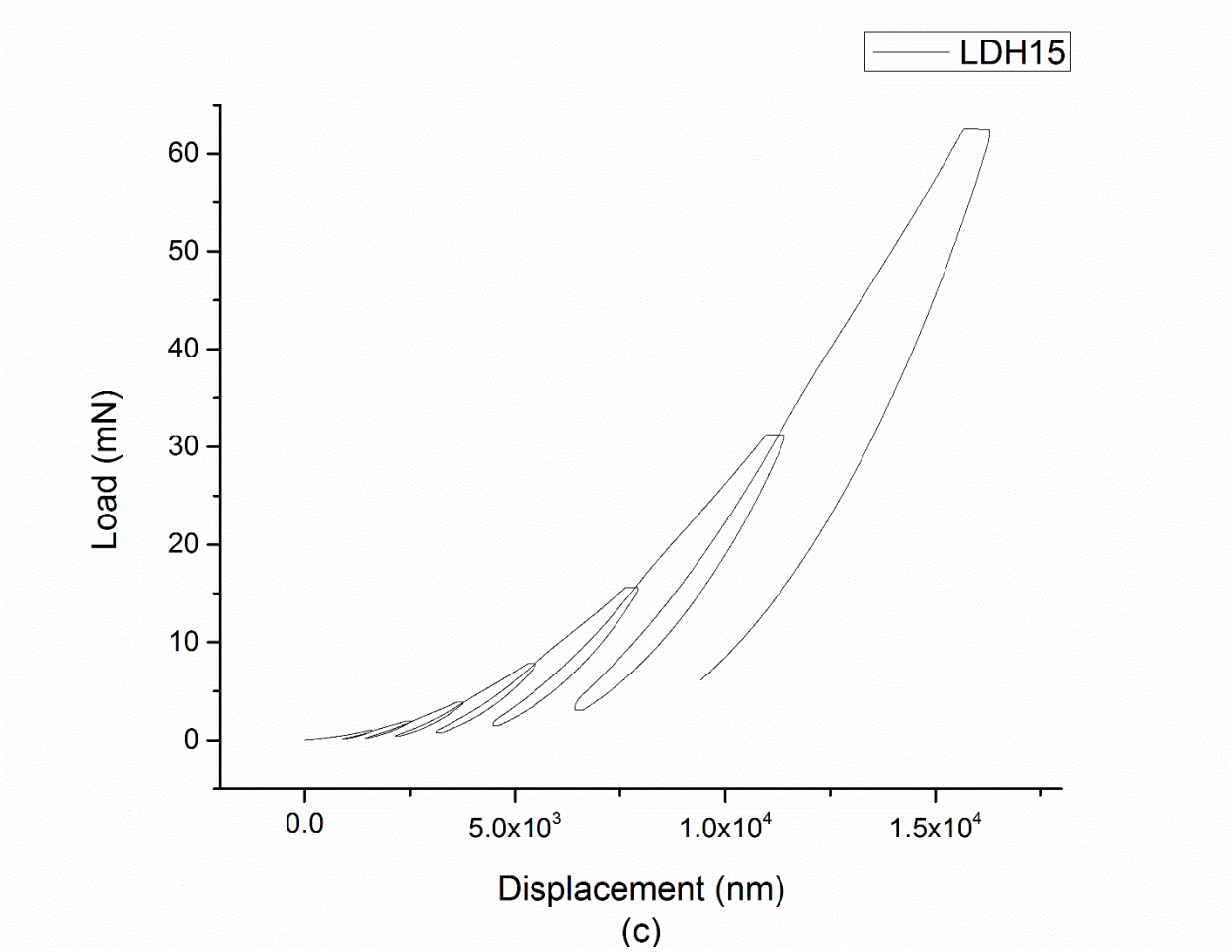

Figure 4. 7(3) Graphical Representation of seven cycle indentation of LDH15.

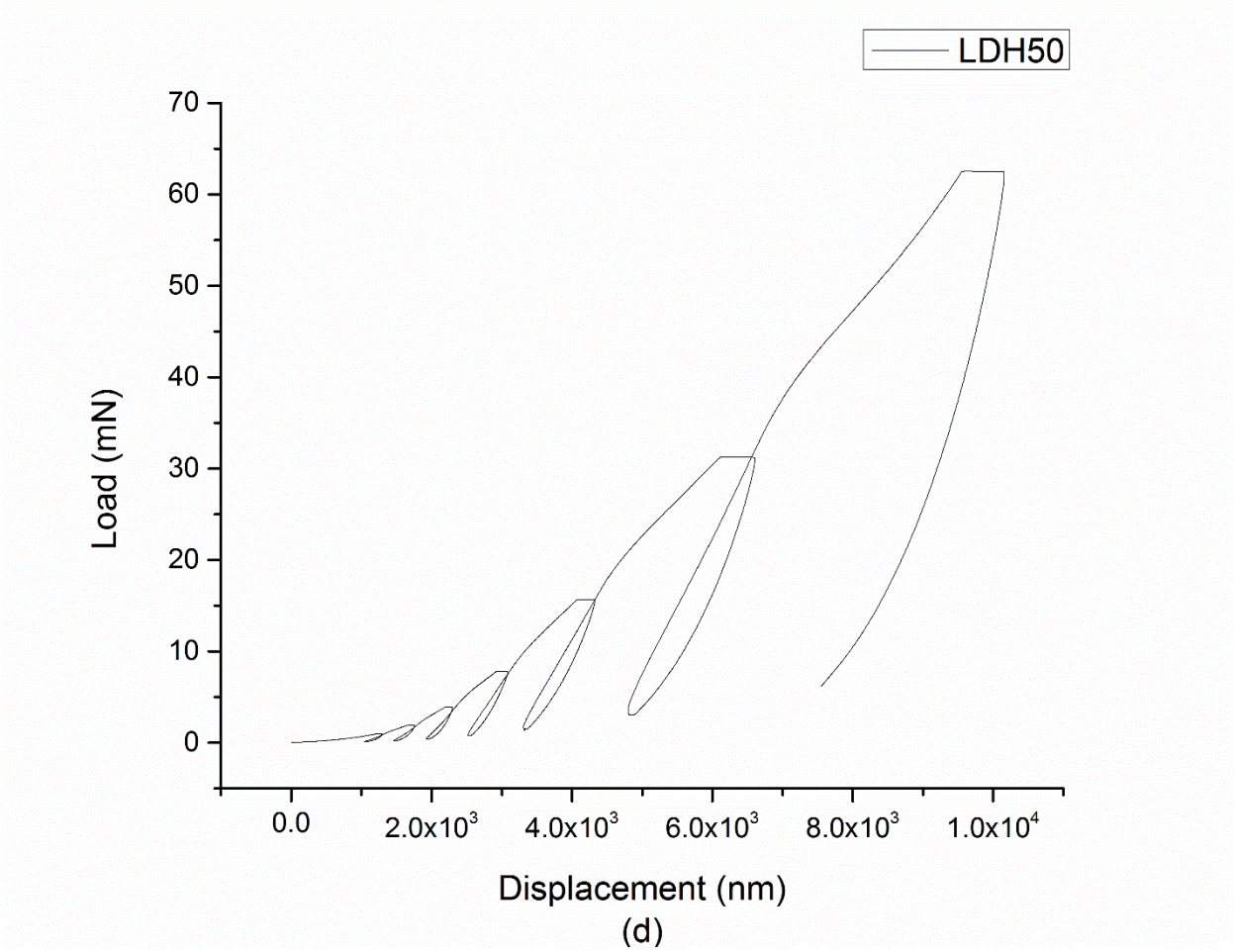

Figure 4. 7(4) Graphical Representation of seven cycle indentation of LDH50.

Also, due to cyclic loading unloading a hysteresis loop is generated as shown in Figure 3.3 which quantify the viscoelasticity of the nanocomposites. It was observed that the absolute viscoelasticity which is given by the area of the hysteresis loop which results due to slow retarded elastic recovery decreases with the addition of LDH, however the relative viscoelasticity which is given as the percent energy loss i.e. the ratio of energy stored by viscoelasticity (EL) to the energy stored due to purely elastic work (ES) increases due to higher percentage of plasticity, Figure 4.8 presents the values of percent energy loss for the nanocomposites coatings.

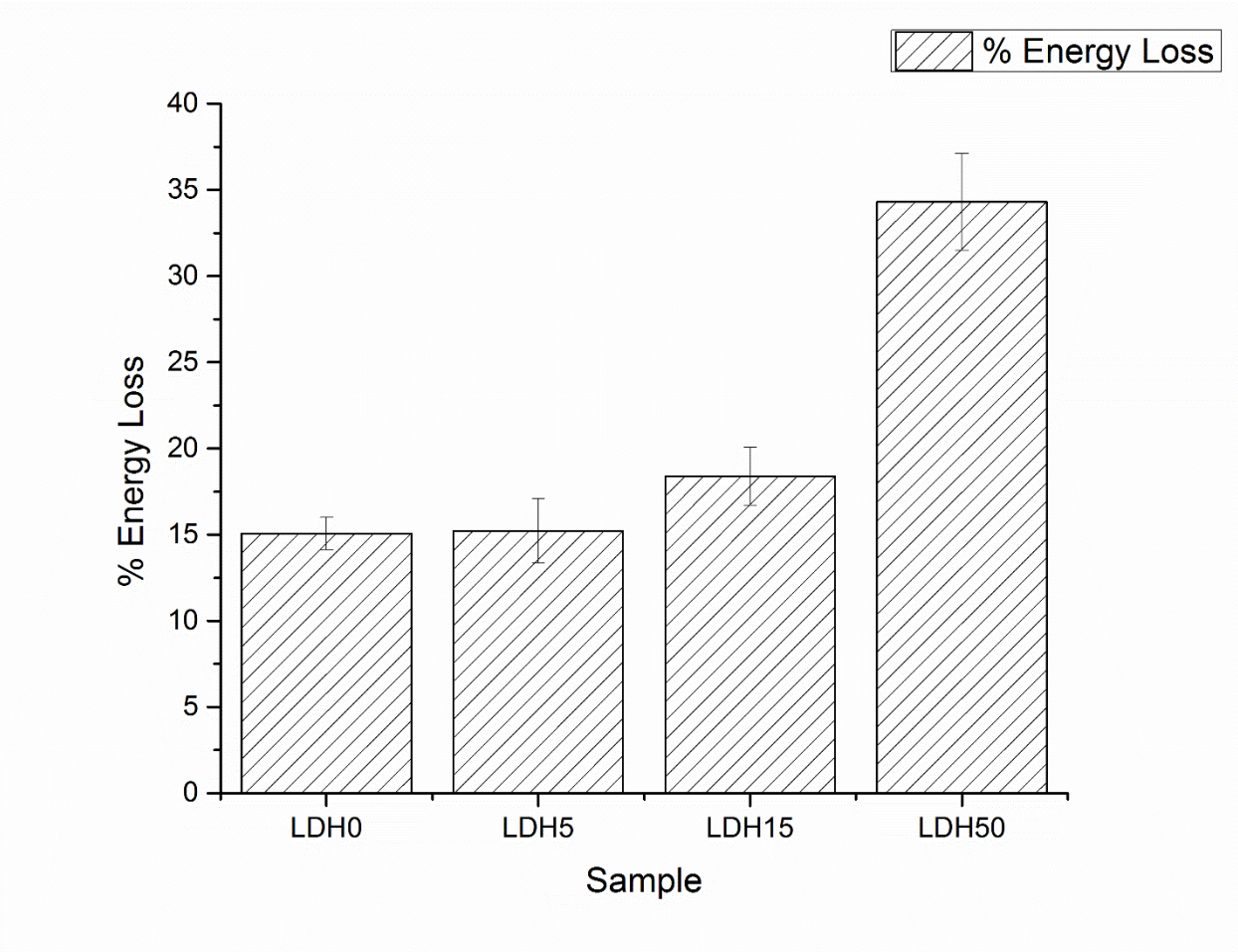

Figure 4. 8 Percent Energy loss (EL/ES) of LDH0, LDH5, LDH15 & LDH50 nanocomposites coatings.

4.4 Differential Scanning Calorimeter (DSC)

The DSC studies revealed the significant thermal properties of the samples, such as crystallinity temperature and melting temperature (Figure 4.9). The table 4.4 shows that the heat of fusion for melting and crystallization decreases with the increase in percentage of LDH moreover the recrystallization temperature in also raised from 60 for neat PBAT to around 100 for LDH50 as the number of nucleating sites are increased raising the crystallization temperature. This effects the optical and physical properties of the nanocomposite and also asserting the heat resistant property. [40] [18]. Table 4.4 also shows that with the addition of LDH, the intensity of heat of fusion and crystallization decreases. Moreover we can also observe a peak shift in the crystallization temperature in the cooling cycle where it's shifted to higher temperatures with the increase of LDH percentage.

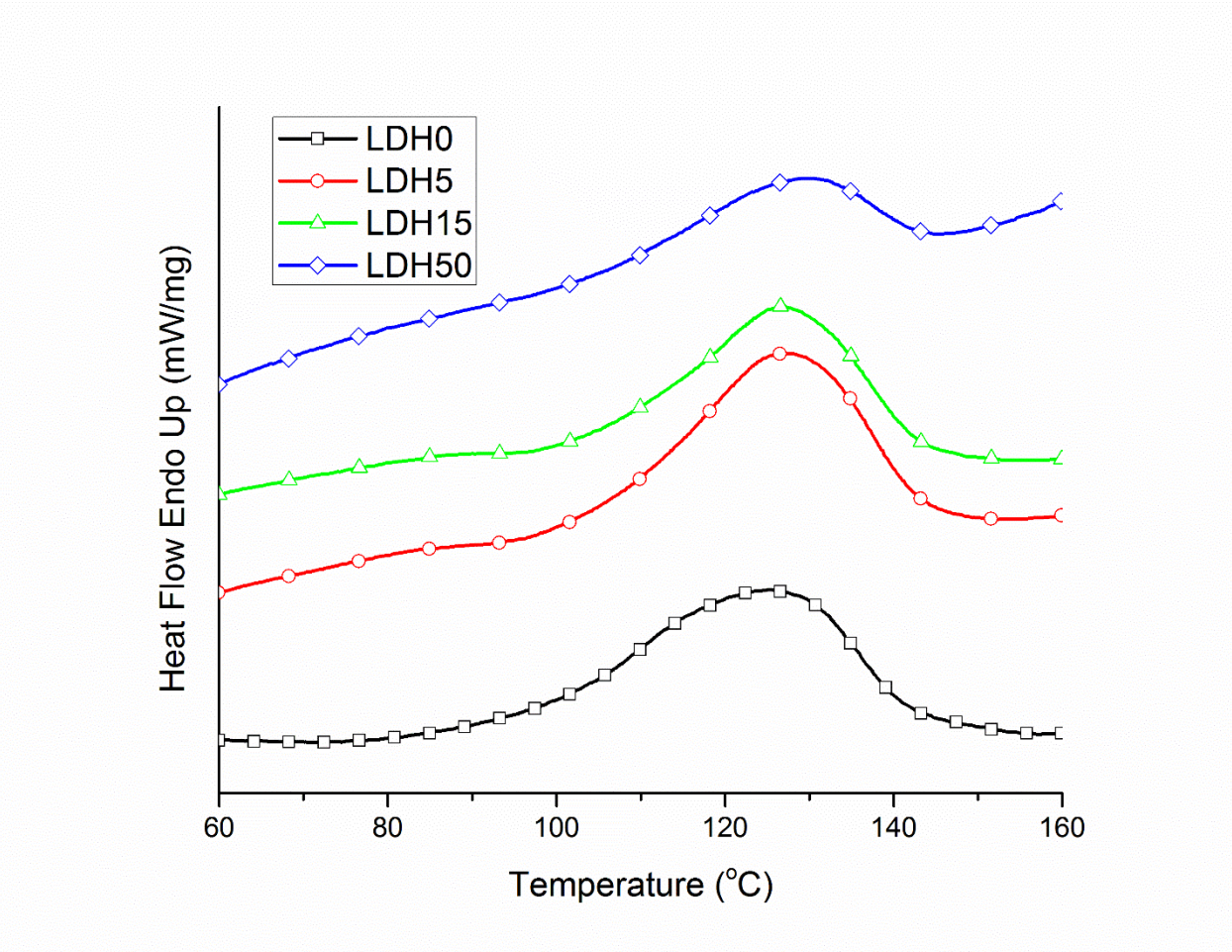

Figure 4. 9(A) DSC second heating curves of pure PBAT and its blend with LDH.

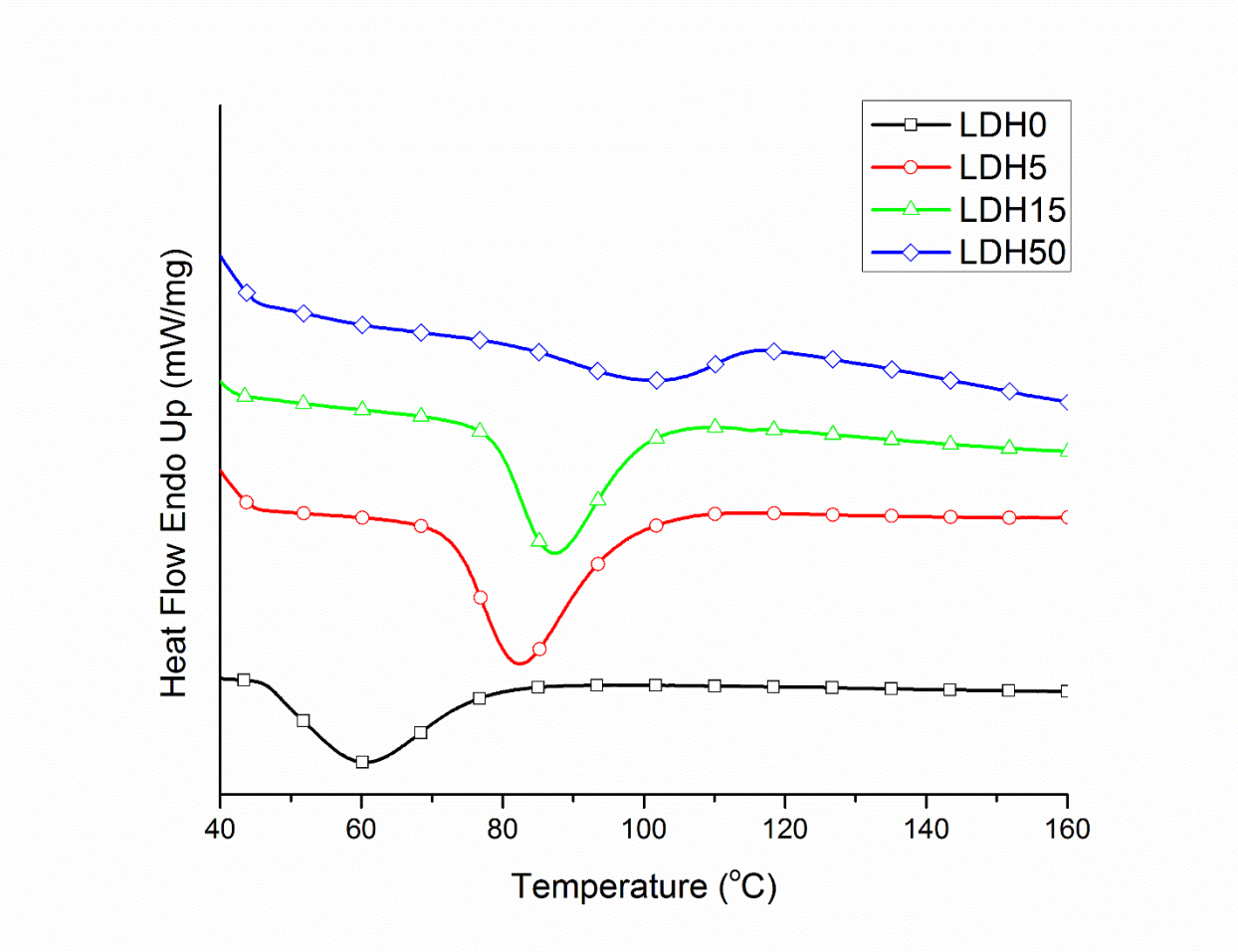

Figure 4. 9(B) DSC second cooling curves of pure PBAT and its bled with LDH

Table 4.4 Experimental Data of Seconding heating and cooling cycle

	Second Heating Cycle		Second Cooling Cycle	
Samples	**T_m (ºC)**	**ΔH (J/g)**	**T_c (ºC)**	**ΔH (J/g)**
LDH0	125.3	13.3	60.4	-23.5
LDH5	126.8	9.0	82.5	-14.2
LDH15	127.4	6.0	87.2	-10.6
LDH50	128.3	3.1	101.4	-2.6

4.5 Scanning Electron Microscope (SEM)

To get the cross-sectional image of the nanocomposite, the sample were fracture in liquid nitrogen to observe the structure that cause an increase in corrosion resistance and enhance modulus and hardness. Image of LDH50 was observe using nanoSEM, from Fig 4.10 the stacking of LDH plates can be observe which is a cause of enhanced mechanical properties and also increase the elastic recovery of the nanocomposites. Moreover the stacking also prevents corrosion as it's provide a zigzag path for the diffusion of ions.

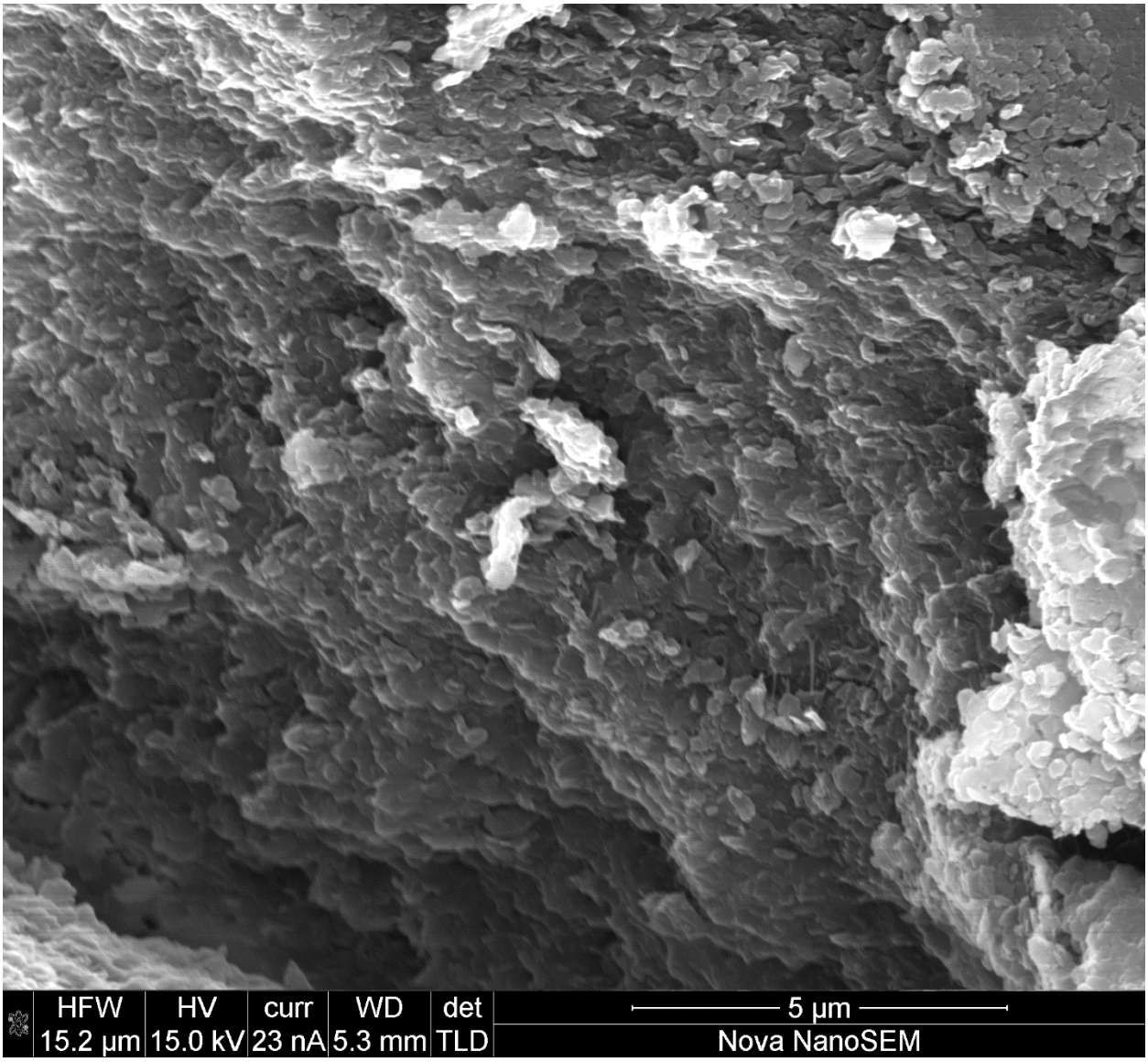

Figure 4. 10 SEM image of LDH50 nanocomposite cross-section.

4.6 Corrosion Resistance Characterization

Overlay potentiodynamic polarization plots of bare; PBAT coated as well as coated samples containing various LDH amounts is shown in Figure 4.11. Corrosion potential (Ecorr) value as shown in Table 5 indicates a shift towards positive values as the percentage of LDH increased. In addition, the corrosion current (Icorr) values decreases with the increase in the percentage of the LDH particles as the stacking of particles causes a zigzag diffusion path for ions to corrode the steel causing a decrease in the corrosion rate. Corrosion resistance efficiency calculated using equation 8 and tabulated in Table 4.5 of the coated steel samples increased with increase in LDH concentration.

$$\%IE = \frac{Bare\ steel\ Icorr - Coated\ steel\ Icorr}{Bare\ steel\ Icorr} \times 100 \ldots\ldots\ldots\ldots (8)$$

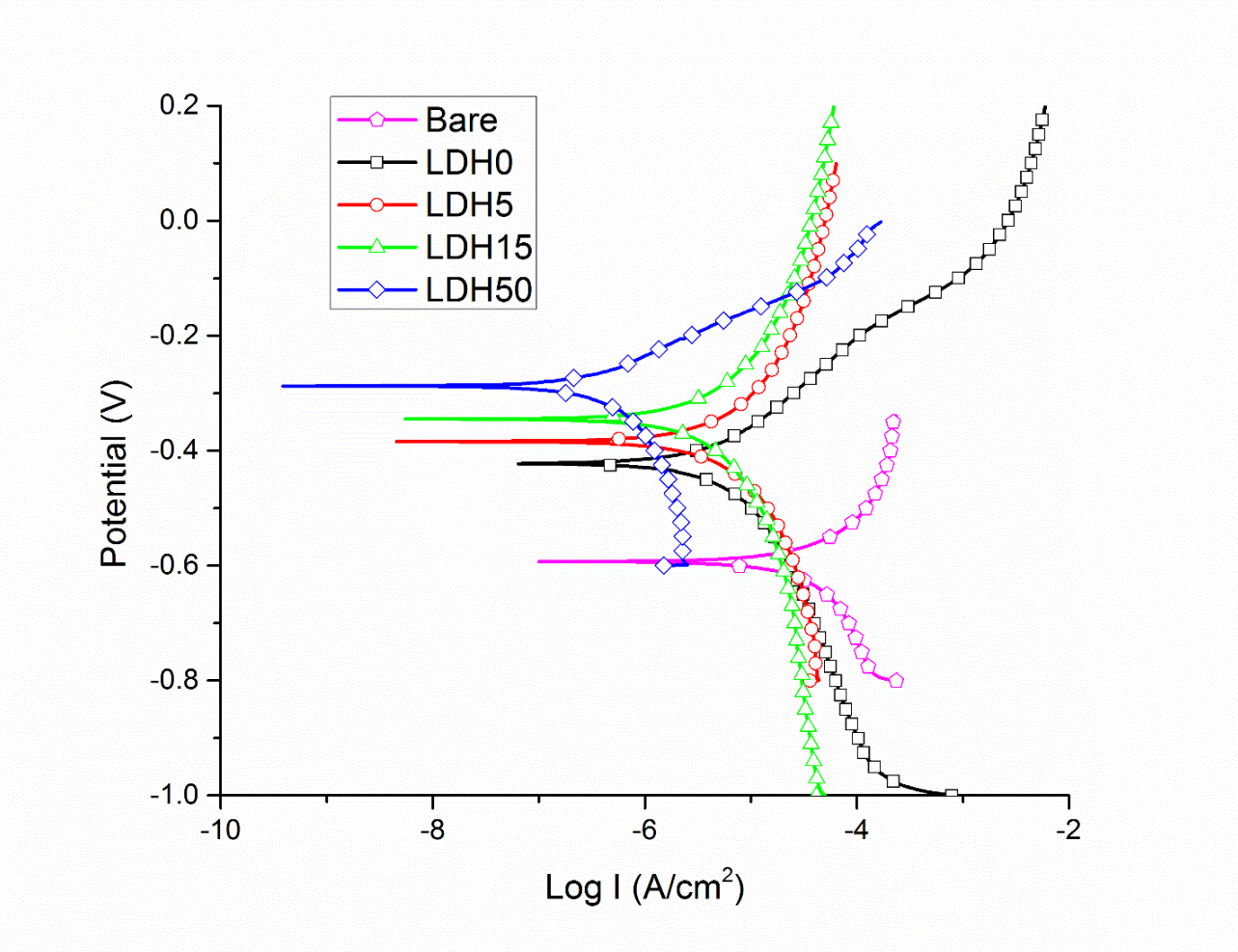

Figure 4. 11 Overlay of Potentiodynamic Polarization plots for bare steel; LDH0, LDH5, LDH15 & LDH50 nanocomposites coatings.

Table 4.5 Value in table based on (± 50 mV) from the open circuit position.

Samples	I corr (μA/cm2)	Ecorr (V)	CR (μm/year)	IE (%)
Bare Steel	20.74	-0.585	242	---
LDH0	4.340	-0.396	50.6	79.09
LDH5	1.832	-0.378	21.3	91.19
LDH15	1.778	-0.341	20.7	91.44
LDH50	0.523	-0.315	6.99	97.11

CHAPTER 5

CONCLUSION

The bioinspired structure that is produced through compression molding with non-solvent modified processing results in a significantly strong, tough, resilient and corrosion resistant coating. Composites showed a 400% increase in modulus. Heat of fusion for melting and crystallization were also decreased with the addition of LDH. Moreover the recrystallization temperature was also raised indicating a heat resistant property. Stacking of the LDH particles also increased corrosion resistance of the polymer as indicated by lower corrosion rates and more positive corrosion potential (Ecorr) values. Nanoindentation results showed that the architecture resulted in increased plasticity of the coating. Representing the increase toughness of the coating inhibiting the propagation of the cracks. Viscoelastic properties were measured using multi cycle nanoindentation. It was observed that the absolute viscoelasticity decreases with the addition of LDH particles which shows the decrease in retarded elastic recovery, however the percent energy loss increases due to the enhance plasticity.

REFERENCES

[1] Sun, Xiao-Yu, Qunyang Li, Yuantong Gu, and Xi-Qiao Feng. 2013. Mechanical properties of bioinspired bicontinuous nanocomposites. Computational Materials Science 80 (0) (12): 71-8.

[2] Zhou, Bin, X. Sherry Liu, Ji Wang, X. Lucas Lu, Aaron J. Fields, and X. Edward Guo. 2014. Dependence of mechanical properties of trabecular bone on plate–rod microstructure determined by individual trabecula segmentation (ITS). Journal of Biomechanics 47 (3) (2/7): 702-8.

[3] Yao, Hong-Bin, Hai-Yu Fang, Zhi-Hua Tan, Li-Heng Wu, and Shu-Hong Yu. 2010. Biologically inspired, strong, transparent, and functional layered organic?inorganic hybrid films. Angewandte Chemie 122 (12): 2186-91.

[4] Li, Yuan-Qing, Ting Yu, Tian-Yi Yang, Lian-Xi Zheng, and Kin Liao. 2012. Bio-inspired nacre-like composite films based on graphene with superior mechanical, electrical, and biocompatible properties. Advanced Materials 24 (25): 3426-31.

[5] Hamed, Elham, and Iwona Jasiuk. 2012. Elastic modeling of bone at nanostructural level. Materials Science and Engineering: R: Reports 73 (3–4) (3/22): 27-49.

[6] Meyers, Marc André, Albert Yu-Min Lin, Po-Yu Chen, and Julie Muyco. 2008. Mechanical strength of abalone nacre: Role of the soft organic layer. Journal of the Mechanical Behavior of Biomedical Materials 1 (1) (1): 76-85.

[7] Weiner, S., and H. D. Wagner. 1998. THE MATERIAL BONE: Structure-mechanical function relations. Annual Review of Materials Science 28 (1) (08/01; 2014/08): 271-98, http://dx.doi.org/10.1146/annurev.matsci.28.1.271.

[8] Wu, Shuilin, Xiangmei Liu, Kelvin W. K. Yeung, Changsheng Liu, and Xianjin Yang. 2014. Biomimetic porous scaffolds for bone tissue engineering. Materials Science and Engineering: R: Reports 80 (0) (6): 1-36.

[9] Darder, M., P. Aranda, and E. Ruiz-Hitzky. 2007. Bionanocomposites: A new concept of ecological, bioinspired, and functional hybrid materials. Advanced Materials 19 (10): 1309-19.

[10] Reddy, Murali M., Singaravelu Vivekanandhan, Manjusri Misra, Sujata K. Bhatia, and Amar K. Mohanty. 2013. Biobased plastics and bionanocomposites: Current status and future opportunities. Progress in Polymer Science 38 (10–11) (0): 1653-89.

[11] Chan Wang et al 2011. A smart multifunctional nanocomposite for intracellular targeted drug delivery and self-release. Nanotechnology 22 415101 doi:10.1088/0957-4484/22/41/415101

[12] Braterman, P.S.; Xu, Z.P.; Yarberry, F. In Handbook of Layered Materials; Auerbach, S.M.;

Carrado, K.A.; Dutta, P.K., Eds.; Marcel Dekker: New York, 2004; p 373-474.

[13] Rives, V., Ed. In Layered Double Hydroxides: Present and Future; Nova Science Publishers: New York 2001; p.1-229.

[14] Whittingham, M.S.; Jacobson. A.J., Eds.; Academic Press: New York, 1982. (ii) Alberti, G.; Costantino, U. In Comprehensive Supramolecular Chemistry; Alberti, G.; Bein, T., Eds.; Wiley: U.K, 1996.

[15] Hule, Rohan A., and Darrin J. Pochan. 2007. Polymer nanocomposites for biomedical applications. MRS Bulletin 32 (04): 354-8, http://dx.doi.org/10.1557/mrs2007.235

[16] Mallakpour, Shadpour, and Mohammad Dinari. 2014. Novel bionanocomposites of poly(vinyl alcohol) and modified chiral layered double hydroxides: Synthesis, properties and a morphological study. Progress in Organic Coatings 77 (3) (3): 583-9.

[17] Sfeir, Charles, Ping-An Fang, Thottala Jayaraman, Aparna Raman, Zhang Xiaoyuan, and Elia Beniash. 2014. Synthesis of bone-like nanocomposites using multiphosphorylated peptides. Acta Biomaterialia 10 (5) (5): 2241-9

[18] Basu, Debdipta, Amit Das, Klaus Werner Stöckelhuber, Udo Wagenknecht, and Gert Heinrich. 2014. Advances in layered double hydroxide (LDH)-based elastomer composites. Progress in Polymer Science 39 (3) (3): 594-626.

[19] Cattalini, J. P., J. García, A. R. Boccaccini, S. Lucangioli, and V. Mouriño. 2013. A new calcium releasing nano-composite biomaterial for bone tissue engineering scaffolds. Procedia Engineering 59 (0): 78-84.

[20] K. L. Dagnon, A. Shaito, S. Ogbomo, S. Ambadapadi, M. Rahimi, V. DeLeon, T. Golden, K. Nguyen, P. Braterman, N. A. D'Souza, "Poly (l-lactic acid) nanocomposites with layer double hydroxides functionalized with Ibuprofen", J. Applied Polym. Sci., 113, 1905–1915 (2009)

[21] DeLeon, Vallerie H., Thanh D. Nguyen, Mangesh Nar, Nandika A. D'Souza, and Teresa D. Golden. 2012. Polymer nanocomposites for improved drug delivery efficiency. Materials Chemistry and Physics 132 (2–3) (2/15): 409-15.

[22] Chrissafis, K., E. Pavlidou, K. M. Paraskevopoulos, T. Beslikas, N. Nianias, and D. Bikiaris. 2011. Enhancing mechanical and thermal properties of PLLA ligaments with fumed silica nanoparticles and montmorillonite. Journal of Thermal Analysis and Calorimetry 105 (1) (07/01): 313-23, http://dx.doi.org/10.1007/s10973-010-1168-z.

[23] Fukushima, Kikku, Amaliya Rasyida, and Ming-Chien Yang. 2013. Characterization, degradation and biocompatibility of PBAT based nanocomposites. Applied Clay Science 80–81 (0) (8): 291-8.

[24] Fukushima, Kikku, Meng-Hsiu Wu, Sergio Bocchini, Amaliya Rasyida, and Ming-Chien Yang. 2012. PBAT based nanocomposites for medical and industrial applications. Materials Science and Engineering: C 32 (6) (8/1): 1331-51.

[25]Ojijo, Vincent, and Suprakas Sinha Ray. 2013. Processing strategies in bionanocomposites. Progress in Polymer Science 38 (10–11) (0): 1543-89.

[26] http://www.doitpoms.ac.uk/tlplib/bones/bone_mechanical.php

[27] S. Vidhate, L. Innocentini-Mei, N. A. D'Souza, "Mechanical and Electrical Multifunctional Poly(3-hydroxybutyrate-co-3-hydroxyvalerate)—Multiwall Carbon Nanotubes Nanocomposites, Polymer Engineering and Science, 52,1367–1374 (2012).

[28] TestWorks® 4 Software for Nanoindentation Systems, Document No. D1418XPA-10629, MANUAL VERSION NO.16

[29] Roche, E. T., Wohlfarth, R., Overvelde, J. T. B., Vasilyev, N. V., Pigula, F. A., Mooney, D. J., Bertoldi, K. and Walsh, C. J. (2014), A Bioinspired Soft Actuated Material. Adv. Mater., 26: 1200–1206. doi:10.1002/adma.201304018

[30] "An improved technique for determining hardness and elastic modulus using load and displacement sensing indentation experiments," W.C. Oliver and G.M. Pharr, Journal of Materials Research, Volume 7, Number 6, pp. 1564 – 1583, June 1992.

[31] "Instrumented indentation testing," J.L. Hay and G.M. Pharr, ASM Handbook, Mechanical Testing and Evaluation, Volume 8, pp. 232-243, October 2000.

[32] Patel, Nimitt G., Arvind Sreeram, Ramaswamy I. Venkatanarayanan, Sitaraman Krishnan, and Philip A. Yuya. 2015. Elevated temperature nanoindentation characterization of poly(para-phenylene vinylene) conjugated polymer films. Polymer Testing 41 (0) (2): 17-25.

[33] Pan, Guanjun, Zhenhua Cao, Mingzhen Wei, Lijun Xu, Jun Shi, and Xiangkang Meng. 2014. Superelasticity of TiNi thin films induced by cyclic nanoindentation deformation at nanoscale. Materials Science and Engineering: A 600 (0) (4/10): 8-11.

[34] Jian, Sheng-Rui. 2015. Pop-in effects and dislocation nucleation of c-plane single-crystal ZnO by berkovich nanoindentation. Journal of Alloys and Compounds 644 (0) (9/25): 54-8.

[35] Trivedi, R., and V. Cech. 2010. Mechanical properties of plasma polymer film evaluated by conventional and alternative nanoindentation techniques. Surface and Coatings Technology 205, Supplement 1 (0) (12/25): S286-9.

[36] Asta Richter, Hubert Gojzewski and Joseph J. Belbruno. 2007. Visco-elastic properties of thin nylon films using multi-cycling nanoindentation. Int. J. Mat. Res. 98 (2007)

[37] Richter, Asta, Michael Gruner, Joseph J. BelBruno, Ursula J. Gibson, and Marek Nowicki. 2006. Nanomechanical measurements on glutamine molecularly imprinted nylon films. Colloids and Surfaces A: Physicochemical and Engineering Aspects 284–285 (0) (8/15): 401-8.

[38] Nanoparticle enhanced conductivity in organic ionic plastic crystals: space charge versus strain induced defect mechanism. - The journal of physical chemistry C.- American Chemical Society.

[39] Wegst, U. G. K., Bai, H., Saiz, E., Tomsia, A. P., & Ritchie, R. O. (2015). Bioinspired structural materials. Nat Mater, 14(1), 23-36. Retrieved from http://dx.doi.org/10.1038/nmat4089

[40] Nerantzaki, Maria, George Z. Papageorgiou, and Dimitrios N. Bikiaris. Effect of nanofiller's type on the thermal properties and enzymatic degradation of poly(ε-caprolactone). Polymer Degradation and Stability(0).